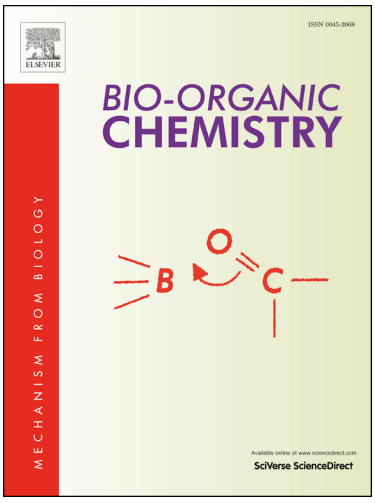

Novel benzotriazole N-acylarylhydrazone hybrids: Design, synthesis, anticancer activity, effects on cell cycle profile, caspase-3 mediated apoptosis and FAK inhibition

Asmaa E. Kassab, Rasha A. Hassan

PII: S0045-2068(18)30420-6
DOI: https://doi.org/10.1016/j.bioorg.2018.07.008
Reference: YBIOO 2427

To appear in: *Bioorganic Chemistry*

Received Date: 29 April 2018
Revised Date: 7 July 2018
Accepted Date: 9 July 2018

Please cite this article as: A.E. Kassab, R.A. Hassan, Novel benzotriazole N-acylarylhydrazone hybrids: Design, synthesis, anticancer activity, effects on cell cycle profile, caspase-3 mediated apoptosis and FAK inhibition, *Bioorganic Chemistry* (2018), doi: https://doi.org/10.1016/j.bioorg.2018.07.008

Novel benzotriazole N-acylarylhydrazone hybrids: Design, synthesis, anticancer activity, effects on cell cycle profile, caspase-3 mediated apoptosis and FAK inhibition

Asmaa E. Kassab [a], Rasha A. Hassan [a]

[a] Pharmaceutical Organic Chemistry Department, Faculty of Pharmacy, Cairo University, Cairo 11562, Egypt.

Address: 33 Kasr El-Aini Street, Cairo, Egypt.

Novel benzotriazole N-acylarylhydrazone hybrids: Design, synthesis, anticancer activity, effects on cell cycle profile, caspase-3 mediated apoptosis and FAK inhibition

Correspondence to: Asmaa E. Kassab, Pharmaceutical Organic Chemistry Department, Faculty of Pharmacy, Cairo University, Cairo 11562, Egypt.

Tel: 002023639307.

Fax: 002023635140.

E-mail: asmaa.kassab@pharma.cu.edu.eg

Abstract

A series of novel benzotriazole N-acylarylhydrazone hybrids was synthesized according fragment-based design strategy. All the synthesized compounds were evaluated for their anticancer activity against 60 human tumor cell lines by NCI (USA). Five compounds: **3d**, **3e**, **3f**, **3o** and **3q** exhibited significant to potent anticancer activity at low concentrations. Compound **3q** showed the most prominent broad-spectrum anticancer activity against 34 tumor cell lines, with mean growth inhibition percent of 45.80%. It exerted the highest potency against colon HT-29 cell line, with cell growth inhibition 86.86%. All leukemia cell lines were highly sensitive to compound **3q**. Additionally, compound **3q** demonstrated lethal activity to MDA-MB-435 belonging melanoma. Compound **3e** exhibited the highest anticancer activity against leukemic CCRF-CEM and HL-60(TB) cell lines, with cell growth

inhibition 86.69% and 86.42%, respectively. Moreover, it exerted marked potency against ovarian OVCAR-3 cancer cell line, with cell growth inhibition 78.24%. Four compounds: **3d**, **3e**, **3f** and **3q** were further studied through determination of IC_{50} values against the most sensitive cancer cell lines. The four compounds exhibited highly potent anticancer activity against ovarian cancer OVCAR-3 and leukemia HL-60 (TB) cell lines, with IC_{50} values in nano-molar range between 25 and 130 nM. They showed 18 to 2.3 folds more potent anticancer activity than doxorubicin. The most prominent compound was **3e**, (IC_{50} values 29 and 25 nM against OVCAR-3 and HL-60 (TB) cell lines, respectively), representing 10 and 18 folds more potency than doxorubicin. The anti-proliferative activity of these four compounds appeared to correlate well with their ability to inhibit FAK at nano-molar range between 44.6 and 80.75 nM. Compound **3e** was a potent, inhibitor of FAK and Pyk2 activity with IC_{50} values of 44.6 and 70.19 nM, respectively. It was 1.6 fold less potent for Pyk2 than FAK. Additionally, it displayed inhibition in cell based assay measuring phosphorylated-FAK (IC_{50} =32.72 nM). Inhibition of FAK enzyme led to a significant increase in the level of active caspase-3, compared to control (11.35 folds), accumulation of cells in pre-G1 phase and annexin-V and propidium iodide staining in addition to cell cycle arrest at G2/M phase indicating that cell death proceeded through an apoptotic mechanism.

Key words: Benzotriazole; N- acylarylhydrazone; Fragment-based design; Synthesis; Anticancer activity; FAK; Caspase-3; Cell cycle arrest profile; Apoptosis.

1. Introduction

One of the vital hallmarks of cancer which distinguishes it from benign tumors is its capability for tissue invasion and distant metastasis [1].

Focal adhesion kinase (FAK) is a multifunctional scaffolding protein tyrosine kinase which is located at specialized subcellular structures known as focal adhesions which link the extracellular matrix to the cytoskeleton. FAK has been shown to be an important mediator of cell adhesion, growth, proliferation, survival, angiogenesis and migration, all of which are often disrupted in cancer cells [2-4]. Furthermore, FAK has anti-apoptotic role via suppression of the activation of caspase-3 that plays pivotal roles in apoptosis [5]. Normal tissues have low expression of FAK, while FAK has been found to be overexpressed in most human cancers, particularly in highly invasive cancer cells [6] such as ovarian cancer [7]. FAK is encoded by the protein tyrosine kinase 2 (PTK2) gene, which is located at human chromosome region 8q24.3. the region was found to be commonly amplified in several types of cancer, such as serous ovarian carcinoma [8]. Therefore, targeting FAK is a rational and novel approach to retard cancer growth and block metastasis [9]. Several FAK inhibitors have been developed and reported recently, such as NVP-TAE-226, PF-562,271, PF-573,228 and FAK Inhibitor 14 (also known as Y15) [10, 11]. These inhibitors have shown activity, either alone or in combination with chemotherapy, both *in vitro* and *in vivo*, against different types of cancer. Additionally, they demonstrated cell cycle arrest in the G2/M phase and subsequently, cellular apoptosis [12]. Strategies targeting FAK inhibition using novel compounds have created an exciting opportunity for anticancer therapy. Benzotriazole is a privileged structure for the design and discovery of novel bioactive molecules and drugs, since it is a structural isostere of purine nucleus, which is found in naturally occurring nucleotides, such as ATP and other naturally existent compounds. Moreover, it has three nitrogen atoms that can act as H-bond acceptors. There-by, benzotriazole derivatives are more ready to bind with catalytic binding sites of a variety of enzymes

and receptors in biological systems, since these ATP binding sites contain specific hydrogen-bond forming groups. In addition, benzotriazole is a common structural motif of marketed anticancer drugs, such as vorozole (Rivizor®) [13] and 4,5,6,7-tetrabromobenzotriazole (TBB) [14] (Figure 1).Compounds I [15] and II [16] (Figure 1) are potent FAK inhibitors. The main structural features of these compounds are benzotriazole ring, substituted at N1 with oxadiazole moiety carrying substituted phenyl ring. N-acylarylhydrazone scaffold,was used as a core to synthesize several anticancer agents as PAC-1 (Figure 1), as it can readily bind with various enzymes and receptors through hydrogen bonds, as well as due to its flexible skeleton [17-19]. The anticancer activity of PAC-1 is dependent on the presence of the *o*-hydroxy N-acylhydrazone motif that played the key role in the chelation of zinc, which is a powerful inhibitor of procaspase-3 enzymatic activity. Such mechanism allows procaspase-3 to process itself to the active form [20-22]. There is an increasing interest in the discovery of lead agents that concomitantly address more than one biological target for cancer treatment [23, 24]. One of the most exciting new methods for lead generation is fragment-based discovery. Fragments are small, low molecular weight molecules that usually form part of drugs (also known as scaffolds or templates). These fragments are then combined or optimized to generate lead compounds [25]. The rational beyond this approach is to identify novel leads with improved affinity and selectivity, [26] and to minimize the drug resistance, as each fragment will have different biological target [27]. Inspired by all these findings, we have constructed a 'hybrid-design' model (Figure 1) to satisfy the pharmacophoric features required to induce FAK inhibition and apoptosis. We have used benzotriazole core to synthesize a series of hybrids substituted at N1 position with biologically active N-acylarylhydrazone scaffold (an apoptosis inducer), moreover, this

scaffold mimics the aryl substituted oxadiazole ring in compounds I and II. In our design strategy, we aimed to incorporate various aryl or heteroaryl groups in the N-acylarylhydrazone core, targeting exploring their impact on anticancer activity and identifying potent anti-proliferative agents. We have introduced mono, di or tri substituted phenyl rings with a diverse array of substitutions, including fluoro, hydroxyl or methoxy groups. We have also incorporated monocyclic heteroaryl moieties [pyrrole, furan or pyridine] or benzo fused heteroaryl rings such as benzofuran, benzothiophene or indole. The anticancer activity of all the newly synthesized compounds was evaluated against a panel of 60 human tumor cell lines provided by National Cancer Institute (USA). Four potent compounds were selected to be further studied through determination of their half maximal inhibitory concentration (IC_{50}) values against ovarian cancer OVCAR-3 and leukemia HL-60 (TB) cell lines. We anticipated that the designed hybrids might be active against different biological targets. In order to explore the mechanistic pathways of the anticancer activity of the synthesized compounds, we chose the most potent compound **3e,** to perform further investigations, such as FAK assay, apoptosis marker (caspase-3) and cell cycle analysis. Molecular docking was performed for compound **3e** to investigate the inhibitor interaction with FAK and explore the binding mode of this compound at the active site.

2. Results and discussion

2.1. Chemistry

Seventeen novel benzotriazole N-acylarylhydrazone derivatives **3a-3q** were synthesized according to Scheme **1**. Commercial benzotriazole was alkylated *via* heating under reflux with an equimolar amount of ethyl chloroacetate in presence of anhydrous K_2CO_3 in dry acetone according to a

reported procedure [28] to give ethyl 2-(1H-benzo[d][1,2,3]triazol-1-yl)acetate (**1**). The C=O stretching of the ester **1** was observed as a strong band at 1747 cm^{-1} in IR spectrum. Heating ester **1** under reflux with three molar equivalents of hydrazine hydrate in ethanol was reported [29] to yield benzotriazole acetohydrazide **2** in 57% yield. IR spectrum of compound **2** showed a decrease in the amidic C=O stretching frequency into 1662 cm^{-1}. New benzotriazole N-acylarylhydrazone derivatives **3a-3q** were prepared through heating under reflux the acetohydrazide **2** with different aromatic aldehydes in ethanol along with a small amount of glacial acetic acid for 6 h. The IR spectra of **3a-3q** showed the amidic C=O stretching as a characteristic strong band in a range (1700-1670 cm^{-1}) and the C=N stretching of the azomethine group (N=CH) as a weak band in the range (1620-1600 cm^{-1}). ^{1}H NMR spectra of these compounds were recorded in DMSO-*d6* and displayed the characteristic signals corresponding to different aryl groups. For all the derivatives **3a-3q**, the ^{1}H NMR spectra showed that the N-acylarylhydrazone is a mixture of two tautomers: tautomer **A** (keto amide) and tautomer **B** (enol amide) (Figure 2). In all the spectra N-CH_2 appeared as two singlet signals at the range of (δ 5.97-6.15 ppm) and the range of (δ 5.57-5.66 ppm) corresponding to tautomer **A** and tautomer **B**, respectively. The integration of these signals was different according to the aromatic substitution and examining the integration pattern of the ^{1}H NMR spectra throughout the seventeen compounds **3a-3q** proved that tautomer **A** was the major in the mixture in all the derivatives. For example, derivative **3b** has two singlets at δ 6.09 ppm and δ 5.63 ppm corresponding to tautomer **A** and tautomer **B**, sequentially with integrations as 2.0 H and 0.50 H. Moreover, the azomethine proton of the hydrazones **3a-3q** appeared in all the ^{1}H NMR spectra as two singlet signals the major at the range (δ 7.92-8.41 ppm) corresponding to tautomer **A** and the minor at the range (δ 8.09-8.62 ppm) corresponding to tautomer **B**. In the ^{1}H NMR spectrum of **3b** the

two singlets were recorded at δ 8.10 ppm and δ 8.30 ppm corresponding to the two tautomeric forms **A** and **B**, respectively with integrations as 1.0 H and 0.25 H. Finally an extra D_2O exchangeable peak appeared in the range (δ 10.0-13.0 ppm) in most of the spectra and was identified as the C-OH in the enol amide (tautomer **B**). For compound **3b**, the D_2O exchangeable peak appeared at δ 12.15 ppm and has integration of 0.25 H. Some of the ^1H NMR spectra of derivatives throughout **3a-3q** showed also peaks corresponding to aromatic protons and the substituents of the phenyl ring of both tautomers **A** and **B**. For example compound **3h** with 4-methoxyphenyl substituent showed the OCH_3 protons as two singlets, at δ 3.82 ppm (3H) and δ 3.81 (0.9H) corresponding to tautomers **A** and **B**, sequentially. Also two singlets at δ 6.04 ppm (2H) and δ 5.59 (0.6 H) corresponding to N-CH_2 protons of **A** and **B**, respectively. The azomethine proton appeared as two singlets at δ 8.04 ppm (1H) and δ 8.23 ppm (0.3H) corresponding to tautomers **A** and **B**, sequentially.^{13}C NMR also supported the presence of tautomeric mixture **A** and **B**. The resonance of the amidic carbonyl in tautomer **A** was at the range (δ 166.8-168.3 ppm) while the enol amide group C(OH)=N corresponding to tautomer **B** appeared as a small peak at the range (δ 161.8-163.3 ppm). Moreover, the N-CH_2 of the two tautomers appeared at the range of (δ 49.1-49.3 ppm) as major peak corresponding to tautomer **A** and at the range (δ 49.5-49.7 ppm) as small peak corresponding to tautomer **B**.

2. 2. Growth inhibition against a panel of 60 human tumor cell lines

In this study, all the newly synthesized compounds were selected by National Cancer Institute (USA) for anticancer evaluation under the Developmental Therapeutic Program (DTP) with respective NCI codes NCS 801617, NCS 801618, NCS 801619, NCS 801620, NCS 801621, NCS 801622, NCS 801623, NCS 801639, NCS 801640, NCS 801641, NCS 801642, NCS 801643, NCS 801644, NCS 801645, NCS 801646,

NCS 801647 and NCS 801648. The selected compounds were evaluated at a single dose (10^{-5} M) against 60 different human tumor cell lines, representing leukemia, melanoma and cancers of lung, colon, central nervous system (CNS), ovary, kidney, prostate as well as breast. The growth inhibition percentages obtained from the single dose test are shown in Table 1. In light of the NCI-60 results, the following observations could be outlined. Compound **3d** exhibited the most potent anticancer activity against ovarian OVCAR-3 and colon HCT-15 cancer cell lines with growth inhibition percentages 71.17 and 70.14, respectively. Regarding compound **3e**, it had mean growth inhibition percent of 53.30%. An interesting phenomenon was that all leukemia cell lines were sensitive to that compound. It exhibited the highest anticancer activity against leukemic CCRF-CEM and HL-60(TB) cell lines with cell growth inhibition 86.69% and 86.42%, sequentially. Moreover, it exerted marked potency against colon HCT-15, melanoma LOX IMVI, ovarian OVCAR-3 and renal UO-31 cancer cell lines with cell growth inhibition percentages 74.21, 77.62, 78.24 and 83.14, respectively. Compound **3f** showed significant to potent cell growth inhibition against the leukemic CCRF-CEM, MOLT-4 and SR cell lines with 66.08%, 62.47% and 64.37% inhibition respectively, the non-small cell lung cancer HOP-62 and NCI-H460 cell lines with 64.81 and 63.54%, the colon cancer COLO 205 and HCT-15 cell lines with 75.23% and 67.85% inhibition respectively. Finally, it showed potent anti-proliferative activity against the ovarian OVCAR-3 cancer cell line with growth inhibition 74%. K-562 and SR cell lines belonging to leukemia were sensitive to compound **3o** with growth inhibition 64.72% and 62.07%, respectively. Compound **3o** revealed the most potent anticancer activity against MDA-MB-435 melanoma cell line with growth inhibition percentage 80.89. It exhibited significant growth inhibition against non-small cell lung cancer NCI-

H522, colon cancer HCT-15, HT29 and breast cancer MCF7cell lines with growth inhibition 68%, 62.26%, 68.76 and 69.27 %, respectively. Compound **3q** showed the most potent anticancer activity at low concentrations against 34 tumor cell lines with mean growth inhibition percent of 45.80%. It exhibited broad spectrum anti-proliferative activity against almost all human cancer types. It is worth mentioning, that all leukemia cell lines were sensitive to compound **3q**. It exerted the highest potency against K-562 cell line with cell growth inhibition 84.79%. It showed selective cell growth inhibition against almost all colon cancer cell lines, HT29 cell line was the most sensitive with 86.86% inhibition. Compound **3q** exhibited potent anti-proliferative activity against lung cancer NCI-H522, melanoma M14, ovarian cancer OVCAR-3 and breast cancer MCF7 cell lines with 81.88%, 80.26%, 77.60% and 77.99% growth inhibition, respectively. Moreover, it showed lethal anticancer activity against MDA-MB-435 melanoma cell line. Compounds (**3a-c**, **3g-n** and **3p**) exhibited no activity against most investigated cell lines.

2.3. Detection of IC_{50} against ovarian cancer OVCAR-3 and leukemia HL-60 (TB) cell lines

Four compounds **3d**, **3e**, **3f** and **3q** were selected to be further studied through determination of their half maximal inhibitory concentration (IC_{50}) values against the most sensitive cancer cell lines compared to doxorubicin as reference anticancer drug. The results of the mean values of experiments performed in triplicate were summarized in Table 2 and represented graphically in Figure 3. The *in vitro* results showed that the four test compounds exhibited highly potent anticancer activity against test cell lines with IC_{50} values in nano molar range between 25 and 130 nM. They showed 18 to 2.3 folds more potent anticancer activity than doxorubicin. The most prominent compound was **3e** with IC_{50} values 29

and 25 nM against OVCAR-3 and HL-60 (TB) cell lines, respectively representing 10 and 18 folds more potency than doxorubicin. Structural activity relationship analysis revealed that the anti-proliferative activity of the newly synthesized hybrids correlates well with the aryl or heteroaryl ring of N-acylhydrazone core. The highly potent compounds were **3d**, **3e**, **3f** and **3q** having the acylhydrazone scaffold with phenyl ring bearing hydroxyl group at ortho position (**3d**, **3e** and **3f**) or having benzene ring with a nearby NH group (**3q**). Such a structural motif is well known with its ability to participate in zinc chelation and consequently is essential for procaspase-3 activation and induction of apoptosis. Further analysis of these compounds clearly revealed that introduction of additional hydroxyl group on the phenyl ring in compounds **3e** and **3f** improved the anticancer activity. Compound **3e** with the additional hydroxyl group at position 3 of phenyl ring showed more potent broad spectrum anticancer activity than compound **3f** with the additional hydroxyl group at position 4. Another interesting phenomenon is that compounds **3a-c** and **3g-j** with phenyl ring substituted with fluoro, hydroxyl or methoxy groups and devoid the presence of ortho hydroxyl group were inactive against most investigated cell lines, confirming that ortho hydroxyl substitution of the phenyl ring is essential for the anticancer activity. Replacement of the phenyl ring of N-acylarylhydrazone core with monoheterocycle in compounds **3k-m** resulted in a dramatic loss in the anti-proliferative activity. Incorporation of a benzo fused heterocycle containing NH group in compound **3q** resulted in broad spectrum and highly potent anticancer activity. According to these findings, we concluded that combination of benzotriazole scaffold with N-acylarylhydrazone core bearing phenyl ring substituted with hydroxyl group at ortho position or having benzene ring with a nearby NH group exerted a positive effect on the anticancer activity.

2.4. Measurement of the effect of benzotriazole hybrids on FAK and Pyk2 enzymes

2.4.1. *In vitro* FAK assay

Benzotriazole scaffold is a part of several potent FAK inhibitors. Therefore, to confirm the FAK binding site as a target, we investigated the inhibitory effect of compounds **3d**, **3e**, **3f** and **3q** on FAK *in vitro*. The anti-proliferative activity of these four compounds appeared to correlate well with their ability to inhibit FAK with IC_{50} values at nano-molar range between 44.6 and 80.75 nM. Compound **3e** showed the most prominent FAK inhibitory activity with IC_{50} = 44.6 ±2.28 nM (Table 3 and Figures 4, 5).

2.4.2. Cell-based FAK auto-phosphorylation assay

To test whether Compound **3e** directly inhibits FAK auto-phosphorylation, we performed *in vitro* kinase assay using FAK (Phospho-Tyr397) Cell-Based ELISA Kit. Compound **3e** displayed inhibition in cell based assay measuring phosphorylated-FAK (IC_{50} =32.72±2.11 nM), which was comparable to GSK-2256098 with IC_{50} value of 20.32 ±1.17 nM.

2.4.3. *In vitro* Pyk2 assay

Since Pyk2 is a tyrosine kinase which is closely related to FAK, both are implicated in cell migration, mitosis and tumor metastasis. We have measured the inhibitory effect of compound **3**e on Pyk2 *in vitro*.

Compound **3e** showed Pyk2 inhibitory activity, at the nanomolar level (IC_{50} value 70.19 ±0.39 nM).

2. 5. Molecular docking of compound 3e in the active site of FAK

Compound **3e** showed highly potent activity in FAK enzyme inhibition assay. At this stage, molecular docking study was carried out to investigate its plausible binding pattern and its interaction with the key amino acids in the active site of FAK. We used the 3D structure of FAK that was downloaded from PDB (ID: 2ETM). The ability of compound **3e** to interact with the key amino acids in the ATP binding site of FAK rationalized its excellent activity. The FAK protein catalytic region formed three interaction bonds with **3e** (Figures 6, 7). As can be seen, compound **3e** interacted by its two OH groups of phenyl ring as H-bond acceptor with the key amino acid Lys 454. Also, N2 of benzotriazole interacted as H-bond acceptor with Cys 502. Moreover, the superior activity of compound **3e** against FAK (IC_{50} value 44.6 nM) was supported by its marked docking score (-13.76 kcal/mol).

2. 6. Effect of compound 3e on the level of active caspase-3 (key executioner of apoptosis)

FAK enzyme has anti-apoptotic role via suppression of the activation of caspase-3. As compound **3e** showed highly potent FAK inhibitory activity at the same time, it contains N-acylarylhydrazone moiety carrying *o*-hydroxyl group, a structural motif known to participate in zinc chelation, which is a powerful inhibitor of procaspase-3 enzymatic activity. So the conversion of procaspase-3 to the active form was suspected as mechanism of action of this compound. The level of active caspase-3 was measured. Treatment of OVCAR-3 cells with compound **3e** at concentration 29 nM produced a significant increase in the level of

active caspase-3 compared to control (11.35 folds) (Table 4 and Figure 8).

2. 7. Cell cycle analysis and detection of apoptosis

The most active compounds **3e** was selected to be further studied regarding to its effect on cell cycle progression and induction of apoptosis in the OVCAR-3 cell line. OVCAR-3 cells were exposed to compound **3e** at its IC_{50} values for 24h and its effect on the normal cell cycle profile and induction of apoptosis was analyzed. Exposure of OVCAR-3 cells to compound **3e** resulted in an interference with the normal cell cycle distribution of this cell line. Compound **3e** induced significant increase in the percentage of cells at pre-G1 by 14 folds, compared to control. Also, it showed significant increase in the percentage of cells at G2/M phases by 5 folds, compared to control (Table 5 and Figures 9, 10). Accumulation of cells in pre-G1 phase which was confirmed by the presence of sub-G1 peaks in the cell cycle profile analysis may result from degradation or fragmentation of the genetic materials confirming a role of apoptosis in compounds **3e** induced cancer cell death and cytotoxicity. While the accumulation of the cells in G2/M phase may result from G2 arrest.

2. 8. Apoptosis determination by Annexin-V assay

To ensure the ability of compound **3e** to induce apoptosis, a biparametric cytofluorimetric analysis was performed using Propidium iodide (PI), which stains DNA and enters only dead cells, and fluorescent immunolabeling of the protein annexin-V, which binds to phosphatidylserine (PS) expressed on the surface of the apoptotic cells and fluoresces green after interacting with the labeled annexin-V [30] . Dual staining for annexin-V and with PI permits discrimination between

live cells, early apoptotic cells, late apoptotic cells and necrotic cells. As shown in Figures 11, 12 and Table 6, after 24 h of treatment of OVCAR-3 cells with compound **3e** at its IC_{50} concentration a decrease in the percentage of the survived cells was observed. Moreover, a significant increase in the percentage of annexin-V positive cells (almost 16 folds more than control) occurred indicating an early apoptosis (lower right quadrant). In addition, some treated cells were in a late apoptotic/ necrotic stage (upper right quadrant). This was indicated by the significant increase in the percentage of annexin V positive, PI positive cells (64 folds more than control).

3. Conclusion

In summary, a series of novel benzotriazole N-acylarylhydrazone hybrids was synthesized according fragment-based design strategy. All the synthesized compounds were evaluated for their anticancer activity by NCI (USA) under DTP. Five compounds **3d**, **3e**, **3f**, **3o** and **3q** exhibited significant to potent anticancer activity at low concentrations. Compounds **3e** and **3q** showed the most potent broad spectrum anti-proliferative activity against several human cancer cell lines. Four compounds **3d**, **3e**, **3f** and **3q** were further studied through determination of IC_{50} values against the most sensitive cancer cell lines. The four compounds exhibited highly potent anticancer activity against ovarian cancer OVCAR-3 and leukemia HL-60 (TB) cell lines with IC_{50} values in nano molar range between 25 and 130 nM. They showed 18 to 2.3 folds more potent anticancer activity than doxorubicin. The most prominent compound was **3e** with IC_{50} values 29 and 25 nM against OVCAR-3 and HL-60 (TB) cell lines, respectively representing 10 and 18 folds more potency than doxorubicin. The anti-proliferative activity of these four compounds appeared to correlate well with their ability to inhibit FAK at

nano-molar range between 44.6 and 80.75 nM. Compound **3e** was a potent, inhibitor of FAK and Pyk2 activity with IC_{50} values of 44.6 and 70.19 nM, respectively. It was 1.6 fold less potent for Pyk2 than FAK. Additionally, it displayed inhibition in cell based assay measuring phosphorylated-FAK (IC_{50}=32.72 nM). Inhibition of FAK enzyme leads to a significant increase in the level of active caspase-3 compared to control (11.35 folds), accumulation of cells in pre-G1 phase and annexin-V and propidium iodide staining in addition to cell cycle arrest at G2/M phase indicating that cell death proceeds through an apoptotic mechanism. Benzotriazole N-acylarylhydrazone hybrids are promising multi-targeted leads for the design and synthesis of potent anticancer agents.

4. Experimental

4. 1. Chemistry

4. 1. 1. General

Melting points were obtained on a Griffin apparatus and were uncorrected. Microanalyses for C, H and N were carried out at the Regional Center for Mycology and Biotechnology, Faculty of Pharmacy, Al-Azhar University. IR spectra were recorded on Shimadzu IR 435 spectrophotometer (Shimadzu Corp., Kyoto, Japan) Faculty of Pharmacy, Cairo University, Cairo, Egypt and values were represented in cm^{-1}. ^{1}H NMR spectra were carried out on Bruker 400 MHz (Bruker Corp., Billerica, MA, USA) spectrophotometer, Faculty of Pharmacy, Cairo University, Cairo, Egypt. Tetramethylsilane (TMS) was used as an internal standard and chemical shifts were recorded in ppm on δ scale and coupling constants (J) were given in Hz. ^{13}C NMR spectra were carried out on Bruker 100 MHz spectrophotometer, Faculty of Pharmacy, Cairo

University, Cairo, Egypt. Progress of the reactions were monitored by TLC using precoated aluminum sheet silica gel MERCK 60F 254 and was visualized by UV lamp.

4. 1. 2. Ethyl 2-(1H-benzo[d][1,2,3]triazol-1-yl)acetate (1)[28]

A mixture of 1H-Benzotriazole (1.0 g, 0.0084 mol), ethyl chloroacetate (1.03 g, 0.0084 mol), anhydrous potassium carbonate (2.32 g, 0.0168 mol) and dry acetone (90 mL) was heated under reflux for 6 h. After cooling the obtained precipitate was filtered, washed with ethanol, and recrystallized from ethanol to afford the ethyl ester **1** as white crystals.

4. 1. 3. 2-(1H-Benzo[d][1,2,3]triazol-1-yl)acetohydrazide (2) [29]

A mixture of the ester **1** (2.05 g, 0.01 mol) and hydrazine hydrate (1.5 g, 0.03 mol) in absolute ethanol (15 mL) was heated under reflux for 5 h. After cooling the obtained precipitate was filtered, washed with water, and recrystallized from ethanol to afford the corresponding hydrazide **2** as white crystals.

4. 1. 4. General procedure for the preparation of compounds (3a-3q)

A mixture of 2-(1H-Benzo[d][1,2,3]triazol-1-yl)acetohydrazide (**2)** (0.2 g, 0.001 mol) and the appropriate aldehyde (0.001 mol) was dissolved in ethanol (5 mL) containing 0.5 mL of glacial acetic acid. The reaction mixture was heated under reflux for 6 h. After cooling the separated solid was filtered, washed with ethanol and crystallized from ethanol.

4. 1. 4. 1. 2-(1H-benzo[d][1,2,3]triazol-1-yl)-N'-(2-fluorobenzylidene) acetohydrazide (3a) white solid: 61 % yield; mp 234-236 ^{o}C; IR (KBr,

cm^{-1}) 3410, 3387, 1685, 1606; ^{1}H NMR (400 MHz, DMSO-d_6) δ 5.63 (s, 0.52 H, N-CH_2 **taut B**), 6.08 (s, 2 H, N-CH_2), 7.29-7.35 (m, 2H, ArH), 7.40-7.44 (m, 1H, ArH), 7.49-7.60 (m, 2H, ArH), 7.84-7.88 (m, 1H, ArH), 8.03-8.05 (m, 2H, ArH), 8.31 (s, 1H, N=CH), 8.51 (s, 0.26H, N=CH, **taut B**), 12.03 (s, 1H, NH, D_2O exchangeable); ^{13}C NMR (100 MHz, DMSO-d_6) δ: 168.0, 162.9 (**taut B**), 161.2 (d, *J*= 248.3) 145.5, 137.8 (d, *J*= 4.6), 134.5, 132.5 (d, *J*= 8.6), 127.7, 127.0, 125.3 (d, *J*= 3.1), 124.3, 121.8 (d, *J*= 9.9), 119.4, 116.4 (d, *J*= 20.5), 111.5, 49.6 (**taut B**), 49.2. Anal. Calcd for $C_{15}H_{12}FN_5O$ (297.29): C, 60.60; H, 4.07; N, 23.56, found C, 60.87; H, 4.19; N, 23.80.

4. 1. 4. 2. 2-(1H-benzo[d][1,2,3]triazol-1-yl)-N'-(3-fluorobenzylidene) acetohydrazide (3b) white solid: 92 % yield; mp 186-188 ^{o}C; IR (KBr, cm^{-1}) 3448, 3421, 1678, 1606; ^{1}H NMR (400 MHz, DMSO-d_6) δ 5.63 (s, 0.50 H, N-CH_2 **taut B**), 6.09 (s, 2 H, N-CH_2), 7.27-7.30 (m, 1H, ArH), 7.40-7.46 (m, 1H, ArH), 7.50-7.61 (m, 3H, ArH), 7.66-7.69 (m, 1H, ArH), 7.84-7.87 (m, 1H, ArH), 8.10 (s, 1H, N=CH), 8.30 (s, 0.25H, N=CH, **taut B**), 11.98 (s, 1H, NH, D_2O exchangeable), 12.15 (s, 0.25H, OH, D_2O exchangeable, **taut B**); ^{13}C NMR (100 MHz, DMSO-d_6) δ: 168.1, 162.9 (**taut B**), 162.8 (d, *J*= 242.2), 145.5, 143.6, 136.9 (d, *J*= 8.0), 134.4, 131.3 (d, *J*= 8.2), 127.3, 124.2, 124.2 (d, *J*= 2.4), 119.4, 118.3, 117.3 (d, *J*= 21.2), 113.3 (d, *J*= 22.6), 111.4, 49.6 (**taut B**), 49.3. Anal. Calcd for $C_{15}H_{12}FN_5O$ (297.29): C, 60.60; H, 4.07; N, 23.56, found C, 60.84; H, 4.21; N, 23.75.

4. 1. 4. 3. 2-(1H-benzo[d][1,2,3]triazol-1-yl)-N'-(4-fluorobenzylidene) acetohydrazide (3c) white solid: 65 % yield; mp 254-255 ^{o}C; IR (KBr, cm^{-1}) 3186, 3167, 1678, 1600; ^{1}H NMR (400 MHz, DMSO-d_6) δ 5.61 (s, 0.55 H, N-CH_2 **taut B**), 6.07 (s, 2 H, N-CH_2), 7.30-7.33 (m, 2H, ArH), 7.40-7.45 (m, 1H, ArH), 7.53-7.60 (m, 1H, ArH), 7.84-7.87 (m, 3H,

ArH), 8.06-8.08 (m, 1H, ArH), 8.09 (s, 1H, N=CH), 8.29 (s, 0.28H, N=CH, **taut B**), 11.89 (s, 1H, NH, D_2O exchangeable), 12.03 (s, 0.26H, OH, D_2O exchangeable, **taut B**). Anal. Calcd for $C_{15}H_{12}FN_5O$ (297.29): C, 60.60; H, 4.07; N, 23.56, found 60.79; H, 4.15; N, 23.78.

4. 1. 4. 4. 2-(1H-benzo[d][1,2,3]triazol-1-yl)-N'-(2-hydroxybenzylidene) acetohydrazide (3d) white solid: 83 % yield; mp 218-220 ^oC; IR (KBr, cm^{-1}) 3387-3100 br s, 3182, 1685, 1608; ^1H NMR (400 MHz, DMSO-d_6) δ 5.63 (s, 1.14H, N-CH_2 **taut B**), 6.03 (s, 2 H, N-CH_2), 6.84-6.89 (m, 1.11H, ArH, **taut B**), 6.90-6.94 (m, 2H, ArH), 7.24-7.24 (m, 0.51H, ArH, **taut B**), 7.27-7.28 (m, 1H, ArH), 7.40-7.44 (m, 1H, ArH), 7.45-7.49 (m, 1H, ArH), 7.53-7.55 (m, 0.55H, ArH, **taut B**), 7.57-7.60 (m, 1H, ArH), 7.77-7.83 (m, 1H, ArH), 7.96 (d, 1H, *J*= 8.4, ArH), 8.06-8.09 (m, 1H, ArH), 8.40 (s, 1H, N=CH), 8.51 (s, 0.54H, N=CH, **taut B**), 10.08 (s, 1H, OH, D_2O exchangeable), 10.88 (s, 0.57H, OH, D_2O exchangeable, **taut B**), 11.83 (s, 1H, NH, D_2O exchangeable). Anal. Calcd for $C_{15}H_{13}N_5O_2$ (295.30): C, 61.01; H, 4.44; N, 23.72, found C, 61.34; H, 4.60; N, 23.91.

4. 1. 4. 5. 2-(1H-benzo[d][1,2,3]triazol-1-yl)-N'-(2,3-dihydroxybenzyl-idene)acetohydrazide (3e) whitish buff solid: 52 % yield; mp 256-258 ^oC; IR (KBr, cm^{-1}) 3271, 3194, 3101, 1670, 1616; ^1H NMR (400 MHz, DMSO-d_6) δ 5.64 (s, 1.25 H, N-CH_2 **taut B**), 6.03 (s, 2 H, N-CH_2), 6.66-6.70 (m, 0.58H, ArH, **taut B**), 6.71-6.75 (m, 1H, ArH), 6.82-6.84 (m, 0.68H, ArH, **taut B**), 6.84-6.86 (m, 1H, ArH), 6.99-7.02 (m, 0.63H, ArH, **taut B**), 7.22-7.28 (m, 1H, ArH), 7.39-7.43 (m, 1H, ArH), 7.45-7.49 (m, 0.62H, ArH, **taut B**), 7.52-7.61 (m, 1H, ArH), 7.86 (d, 1H, *J*= 8.4, ArH), 7.94-7.97 (m, 0.61H, ArH, **taut B**), 8.05-8.09 (m, 1H, ArH), 8.40 (s, 1H, N=CH), 8.46 (s, 0.63H, N=CH, **taut B**), 9.36 (br s, 2H, OH, D_2O exchangeable), 10.54 (s, 0.62H, OH, D_2O exchangeable, **taut B**), 11.81 (s, 1H, NH, D_2O exchangeable); ^{13}C NMR (100 MHz, DMSO-d_6) δ:

167.4, 162.6 (**taut B**), 1489.9, 146.1, 145.8, 145.5, 142.9, 134.5, 127.9, 127.6, 124.4, 124.2, 121.0,, 119.6,119.5, 119.4,112.1, 111.5, 49.5 (**taut B**), 49.2. Anal. Calcd for $C_{15}H_{13}N_5O_3$ (311.30): C, 57.87; H, 4.21; N, 22.50, found C, 58.13; H, 4.34; N, 22.74.

4. 1. 4. 6. 2-(1H-benzo[d][1,2,3]triazol-1-yl)-N'-(2,4-dihydroxybenzyl-idene)acetohydrazide (3f) white solid: 53 % yield; mp 276-277 ^{o}C; IR (KBr, cm^{-1}) 3182, 3101, 3066, 1678, 1627; ^{1}H NMR (400 MHz, DMSO-d_6) δ 5.60 (s, 1.45 H, N-CH_2 **taut B**), 5.99 (s, 2 H, N-CH_2), 6.30-6.32 (m, 1.40H, ArH, **taut B**), 6.34-6.36 (m, 2H, ArH), 7.34-7.37 (m, 0.72H, ArH, **taut B**), 7.39-7.43 (m, 1H, ArH), 7.52-7.56 (m, 1H, ArH), 7.58-7.60 (m, 1H, ArH), 7.85 (d, 1H, *J*=8.4, ArH), 8.05-8.09 (m, 1H, ArH), 8.27 (s, 1H, N=CH), 8.37 (s, 0.7H, N=CH, **taut B**), 9.88 (s, 1H, OH, D_2O exchangeable), 9.98 (s, 1H, OH, D_2O exchangeable), 11.02 (s, 0.70H, OH, D_2O exchangeable, **taut B**), 11.60 (s, 1H, NH, D_2O exchangeable), 11.99 (s, 0.69H, OH, D_2O exchangeable, **taut B**). Anal. Calcd for $C_{15}H_{13}N_5O_3$ (311.30): C, 57.87; H, 4.21; N, 22.50, found C, 57.98; H, 4.39; N, 22.81.

4. 1. 4. 7. 2-(1H-benzo[d][1,2,3]triazol-1-yl)-N'-(3,4-dihydroxybenzyl-idene)acetohydrazide (3g) white solid: 57 % yield; mp 276-278 ^{o}C; IR (KBr, cm^{-1}) 3479-3417,3298, 1678, 1612; ^{1}H NMR (400 MHz, DMSO-d_6) δ 5.57 (s, 0.66 H, N-CH_2 **taut B**), 6.01 (s, 2 H, N-CH_2), 6.77 (s, 0.36H, ArH, **taut B**), 6.81 (d, 1H, *J*=8.4, ArH), 6.93-6.96 (m, 0.33H, ArH, **taut B**), 6.99-7.01 (m, 1H, ArH), 7.22 (s, 0.33H, ArH, **taut B**), 7.25 (s, 1H, ArH), 7.39-7.45 (m, 1H, ArH), 7.52-7.59 (m, 1H, ArH), 7.86 (d, 1H, *J*=8.4, ArH), 7.93 (s, 1H, N=CH), 8.06-8.08 (m, 1H, ArH), 8.09 (s, 0.35H, N=CH, **taut B**), 9.43 (brs, 2H, OH, D_2O exchangeable), 11.62 (s, 1H, NH, D_2O exchangeable); ^{13}C NMR (100 MHz, DMSO-d_6) δ: 167.3, 162.2 (**taut B**), 148.4, 146.1, 145.7, 145.5, 134.5, 127.7, 125.7, 124.2,

120.7, 119.4, 116.0, 113.4, 111.5, 49.6 (**taut B**), 49.1. Anal. Calcd for $C_{15}H_{13}N_5O_3$ (311.30): C, 57.87; H, 4.21; N, 22.50, found C, 57.93; H, 4.45; N, 22.72.

4. 1. 4. 8. 2-(1H-benzo[d][1,2,3]triazol-1-yl)-N'-(4-methoxybenzylidene)acetohydrazide (3h) white solid: 88 % yield; mp 196-198 ^{o}C; IR (KBr, cm^{-1}) 3444, 3421, 3190, 1678, 1604; ^{1}H NMR (400 MHz, DMSO-d_6) δ 3.81 (s, 0.9H, OCH_3, **taut B**), 3.82 (s, 3H, OCH_3), 5.59 (s, 0.6H, N-CH_2 **taut B**), 6.04 (s, 2 H, N-CH_2), 7.00-7.04 (m, 2H, ArH), 7.40-7.43 (m, 1H, ArH), 7.53-7.60 (m, 1H, ArH), 7.69-7.74 (m, 2H, ArH), 7.83-7.87 (m, 1H, ArH), 8.04 (s, 1H, N=CH), 8.06-8.09 (m, 1H, ArH), 8.23 (s, 0.3H, N=CH, **taut B**), 11.76 (s, 1H, NH, D_2O exchangeable), 11.87 (s, 0.29 H, OH, D_2O exchangeable, **taut B**); ^{13}C NMR (100 MHz, DMSO-d_6) δ: 167.5, 162.4 (**taut B**), 161.3, 145.5, 145.0, 144.9, 134.5, 129.3, 129.1, 127.7, 126.8, 124.2, 119.4, 118.3, 114.8, 114.7, 111.5, 55.7, 49.6 (**taut B**), 49.2. Anal. Calcd for $C_{16}H_{15}N_5O_2$ (309.33): C, 62.13; H, 4.89; N, 22.64, C, found 62.40; H, 5.03; N, 22.78.

4. 1. 4. 9. 2-(1H-benzo[d][1,2,3]triazol-1-yl)-N'-(4-hydroxy-3-methoxybenzylidene) acetohydrazide (3i) white solid: 75 % yield; mp 242-244 ^{o}C; IR (KBr, cm^{-1}) 3224, 3159, 1693, 1606; ^{1}H NMR (400 MHz, DMSO-d_6) δ 3.80 (s, 0.9H, OCH_3, **taut B**), 3.84 (s, 3H, OCH_3), 5.58 (s, 0.61H, N-CH_2 **taut B**), 6.05 (s, 2 H, N-CH_2), 6.83-6.85 (m, 1H, ArH), 7.12-7.15 (m, 1H, ArH), 7.39-7.43 (m, 2H, ArH), , 7.53-7.60 (m, 1H, ArH), 7.83-7.87 (m, 1H, ArH), 7.97 (s, 1H, N=CH), 8.06-8.08 (m, 1H, ArH), 8.16 (s, 0.3H, N=CH, **taut B**), 9.58 (br s, 1H, OH, D_2O exchangeable), 11.70 (s, 1H, NH, D_2O exchangeable). Anal. Calcd for $C_{16}H_{15}N_5O_3$ (325.33): C, 59.07; H, 4.65; N, 21.53, found C, 59.31; H, 4.82; N, 21.79.

4. 1. 4. 10. 2-(1H-benzo[d][1,2,3]triazol-1-yl)-N'-(3,4,5-trimethoxybenzylidene)acetohydrazide (3j) white solid: 94 % yield; mp 213-214 ^{o}C;

IR (KBr, cm^{-1}) 3425, 3186, 1685, 1616 ; ^1H NMR (400 MHz, DMSO-d_6) δ 3.70 (s, 0.88H, OCH_3, **taut B**), 3.71 (s, 3H, OCH_3), 3.82 (s, 1.57H, OCH_3), **taut B**), 3.85 (s, 6H, 2(OCH_3)), 5.61 (s, 0.57 H, N-CH_2 **taut B**), 6.09 (s, 2 H, N-CH_2), 7.11 (s, 2H, ArH), 7.40-7.44 (m, 1H, ArH), 7.45-7.48 (m, 0.53H, ArH, **taut B**), 7.53-7.60 (m, 1H, ArH), 7.83-7.88 (m, 1H, ArH), 8.01 (s, 1H, N=CH), 8.06-8.09 (m, 1H, ArH), 8.21 (s, 0.27H, N=CH, **taut B**), 11.94 (s, 1H, NH, D_2O exchangeable); ^{13}C NMR (100 MHz, DMSO-d_6) δ: 167.8, 162.7 (**taut B**), 153.6, 145.5, 144.9, 139.6, 134.4, 129.8, 127.7, 124.3, 119.4, 111.4, 104.8, 60.6, 56.4, 49.6 (**taut B**), 49.3. Anal. Calcd for $C_{18}H_{19}N_5O_4$ (369.38): C, 58.53; H, 5.18; N, 18.96, found C, 58.26; H, 5.40; N, 19.23.

4. 1. 4. 11. 2-(1H-benzo[d][1,2,3]triazol-1-yl)-N'-(furan-2-ylmethylene) acetohydrazide (3k) white solid: 63% yield; mp 216-217 ^oC; IR (KBr, cm^{-1}) 3228, 3170, 1793, 1670, 1616; ^1H NMR (400 MHz, DMSO-d_6) δ 5.60 (s, 0.67 H, N-CH_2 **taut B**), 5.97 (s, 2 H, N-CH_2), 6.66-6.67 (m, 1H, ArH), 6.98 (d, 1H, *J*=3.2, ArH), 7.39-7.45 (m, 1H, ArH), 7.52-7.99 (m, 1H, ArH), 7.83-7.87 (m, 2H, ArH), 7.99 (s, 1H, N=CH), 8.05-8.09 (m, 1H, ArH), 8.17 (s, 0.33H, N=CH, **taut B**), 11.93 (s, 1H, NH, D_2O exchangeable). Anal. Calcd for $C_{13}H_{11}N_5O_2$ (269.26): C, 57.99; H, 4.12; N, 26.01, found C, 58.13; H, 4.39; N, 26.25.

4. 1. 4. 12. N'-((1H-pyrrol-2-yl)methylene)-2-(1H-benzo[d][1,2,3]triazol-1-yl)acetohydrazide (3l) white solid: 70 % yield; mp 264-265 ^oC; IR (KBr, cm^{-1}) 3190, 3101, 1678, 1620; ; ^1H NMR (400 MHz, DMSO-d_6) δ 5.57 (s, 0.69 H, N-CH_2 **taut B**), 6.03 (s, 2 H, N-CH_2), 6.13-6.17 (m, 1H, ArH), 6.49-6.52 (m, 1H, ArH), 6.99-7.00 (m, 1H, ArH), 7.40-7.44 (m, 1H, ArH), 7.53-7.58 (m, 1H, ArH), 7.81-7.86 (m, 1H, ArH), 7.92 (s, 1H, N=CH), 8.07 (d, 1H, *J*=8.4, ArH), 8.12 (s, 0.34 H, N=CH, **taut B**), 11.47

(s, 1H, NH, D_2O exchangeable), 11.52 (s, 0.38 H, NH, D_2O exchangeable, **taut B**), 11.99 (s, 1H, NH, D_2O exchangeable), 11.69 (s, 0.35 H, OH, D_2O exchangeable, **taut B**). Anal. Calcd for $C_{13}H_{12}N_6O$ (268.28): C, 58.20; H, 4.51; N, 31.33, found C, 58.02; H, 4.83; N, 31.61.

4. 1. 4. 13. 2-(1H-benzo[d][1,2,3]triazol-1-yl)-N'-(pyridin-4-ylmethylene) acetohydrazide (3m) White solid: 92 % yield; mp 230-231 ^oC; IR (KBr, cm^{-1}) 3132, 1701, 1600; ^1H NMR (400 MHz, DMSO-d_6) δ 5.66 (s, 0.46 H, N-CH_2 **taut B**), 6.12 (s, 2 H, N-CH_2), 7.40-7044 (m, 1H, ArH), 7.45-7.48 (m, 1H, ArH), 7.52-7.60 (m, 1H, ArH), 7.65-7.67 (m, 0.46H, ArH, **taut B**), 7.71-7.76 (m, 2H, ArH), 7.84-7.88 (m, 1H, ArH), 8.08 (s, 1H, N=CH), 8.29 (s, 0.23H, N=CH, **taut B**), 7.65 (d, 0.47H, ArH, **taut B**), 8.66-8.68 (m, 2H, ArH), 12.16 (s, 1H, NH, D_2O exchangeable), 12.30 (s, 0.23H, OH, D_2O exchangeable, **taut B**). ^{13}C NMR (100 MHz, DMSO-d_6) δ: 168.3, 163.2 (**taut B**), 150.6, 145.5, 144.5, 142.5, 141.5, 134.5, 127.7, 126.9, 124.2, 121.4, 119.4, 118.3, 111.4, 49.7 (**taut B**), 49.3. Anal. Calcd for $C_{14}H_{12}N_6O$ (280.29): C, 59.99; H, 4.32; N, 29.98, found C, 59.72; H, 4.59; N, 29.73.

4. 1. 4. 14. 2-(1H-benzo[d][1,2,3]triazol-1-yl)-N'-(benzofuran-2-ylmethy- lene)acetohydrazide (3n) white solid: 57 % yield; mp 199-200 ^oC; IR (KBr, cm^{-1}) 3221, 3178, 1685, 1620; ^1H NMR (400 MHz, DMSO-d_6) δ 5.66 (s, 0.65 H, N-CH_2 **taut B**), 6.06 (s, 2 H, N-CH_2), 7.32 (t, 1H, *J*=6.4, ArH), 7.40 (s, 0.99H, ArH, **taut B**), 7.42-7.46 (m, 3H, ArH), 7.55-7.57 (m, 1H, ArH), 7.64-7.68 (m, 1H, ArH), 7.71-7.74 (m, 1H, ArH), 7.86 (d, 0.32H, *J*=8.4, ArH, **taut B**), 7.89 (d, 1H, *J*=8.4, ArH), 7.95-7.97 (m, 0.32H, ArH, **taut B**), 8.06-8.10 (m, 1H, ArH), 8.14 (s, 1H, N=CH), 8.32 (s, 0.32H, N=CH, **taut B**), 12.16 (s, 1H, NH, D_2O exchangeable); ^{13}C NMR (100 MHz, DMSO-d_6) δ: 167.9, 163.0 (**taut B**), 155.1, 151.1, 145.5, 135.1, 134.6, 128.1, 127.7, 126.8, 124.2, 124.0, 122.4, 119.4,

111.8, 111.6, 111.0, 49.7 (**taut B**), 49.1. Anal. Calcd for $C_{17}H_{13}N_5O_2$ (319.32): C, 63.94; H, 4.10; N, 21.93, found C, 64.21; H, 4.28; N, 22.15.

4. 1. 4. 15. N'-(benzo[b]thiophen-2-ylmethylene)-2-(1H-benzo[d][1,2,3]-triazol-1-yl)acetohydrazide (3o) yellowish white solid: 89 % yield; mp 220-222 ^{o}C; IR (KBr, cm^{-1}) 3421, 3367, 1685, 1608; ^{1}H NMR (400 MHz, DMSO-d_6) δ 5.63 (s, 0.74 H, N-CH_2 **taut B**), 6.01 (s, 2 H, N-CH_2), 7.41-7.44 (m, 3H, ArH), 7.54-7.61 (m, 1H, ArH), 7.83-7.90 (m, 3H, ArH), 7.95-7.97 (m, 1H, ArH), 8.06-8.10 (m, 1H, ArH), 8.41 (s, 1H, N=CH), 8.62 (s, 0.38H, N=CH, **taut B**), 12.04 (s, 1H, NH, D_2O exchangeable), 12.15 (s, 0.23H, OH, D_2O exchangeable, **taut B**). Anal. Calcd for $C_{17}H_{13}N_5OS$ (335.39): C, 60.88; H, 3.91; N, 20.88, found C, 60.72; H, 4.12; N, 20.72.

4. 1. 4. 16. N'-((1H-indol-2-yl)methylene)-2-(1H-benzo[d][1,2,3]triazol-1-yl)acetohydrazide (3p) whitish buff solid: 79 % yield; mp 281-282 ^{o}C; IR (KBr, cm^{-1}) 3286, 3221, 3178, 1685, 1608 ; ^{1}H NMR (400 MHz, DMSO-d_6) δ 5.63 (s, 0.52 H, N-CH_2 **taut B**), 6.15 (s, 2 H, N-CH_2), 6.87 (s, 1H, ArH), 7.01-7.06 (m, 1H, ArH), 7.20 (t, 1H, *J*=7.6 ArH), 7.42-7.49 (m, 2H, ArH), 7.55-7.60 (m, 2H, ArH), 8.89 (d, 1H, *J*=8.4, ArH), 8.08 (d, 1H, *J*=8.4, ArH), 8.12 (s, 1H, N=CH), 8.33 (s, 0.28H, N=CH, **taut B**), 11.50 (s, 1H, NH, D_2O exchangeable), 11.56 (s, 0.27H, NH, D_2O exchangeable, **taut B**), 11.94 (s, 1H, NH, D_2O exchangeable). Anal. Calcd for $C_{17}H_{14}N_6O$ (318.34): C, 64.14; H, 4.43; N, 26.40, found C, 64.35; H, 4.59; N, 26.81.

4. 1. 4. 17. N'-((1H-indol-3-yl)methylene)-2-(1H-benzo[d][1,2,3]triazol-1-yl)acetohydrazide (3q) white solid: 86 % yield; mp 253-255 ^{o}C; IR (KBr, cm^{-1}) 3248, 3228, 3190, 1670, 1616; ; ^{1}H NMR (400 MHz, DMSO-

d_6) δ 5.58 (s, 0.45 H, N-CH_2 **taut B**), 6.09 (s, 2 H, N-CH_2), 7.14-7.24 (m, 2H, ArH), 7.40-7.48 (m, 2H, ArH), 7.53-7.57 (m, 1H, ArH), 7.85-7.90 (m, 2H, ArH), 8.08 (d, 1H,*J*=8.8, ArH), 8.25-8.27 (m, 1H, ArH), 8.29 (s, 1H, N=CH), 8.45 (s, 0.23H, N=CH, **taut B**), 11.56 (s, 1H, NH, D_2O exchangeable), 11.61 (s, 1H, NH, D_2O exchangeable), 11.68 (s, 0.23H, OH, D_2O exchangeable, **taut B**); ^{13}C NMR (100 MHz, DMSO-d_6) δ: 166.8, 161.8 (**taut B**), 145.5, 142.6, 137.5, 134.5, 131.3, 127.7, 124.4, 124.3, 123.1, 122.3, 121.2, 119.4, 112.3, 111.6, 111.6, 49.7 (**taut B**), 49.2. Anal. Calcd for $C_{17}H_{14}N_6O$ (318.34): C, 64.14; H, 4.43; N, 26.40, found C, 64.42; H, 4.65; N, 26.67.

4. 2. Anticancer activity

4. 2. 1. Measurement of anticancer activity against a panel of 60 cell lines

Anticancer activity screening of the newly synthesized compounds was measured *in vitro* utilizing 60 different human tumor cell lines provided by US National Cancer Institute according to previously reported standard procedure [31-33] as follows: Cells are inoculated into 96-well microtiter plates in 100 mL. After cell inoculation, the microtiter plates are incubated at 37 °C, 5% CO_2, 95% air and 100% relative humidity for 24 h prior to addition of experimental compounds. After 24 h, two plates of each cell line are fixed in situ with TCA, to represent a measurement of the cell population for each cell line at the time of drug addition (Tz).

Experimental compounds are solubilized in dimethyl sulfoxide at 400-fold the desired final maximum test concentration and stored frozen prior to use. At the time of compound addition, an aliquot of frozen concentrate is thawed and diluted to twice the desired final maximum test concentration with complete medium containing 50 mg/mL gentamicin. Aliquots of 100 mL of the compounds dilutions are added to the appropriate microtiter wells already containing 100 mL of medium, resulting in the required final compound concentration. Following compound addition, the plates are incubated for an additional 48 h at 37 ^{o} C, 5% CO_2, 95% air, and 100% relative humidity. For adherent cells, the assay is terminated by the addition of cold trichloroacetic acid (TCA). Cells are fixed in situ by the gentle addition of 50 mL of cold 50% (w/v) TCA (final concentration, 10% TCA) and incubated for 60 minutes at 4 ^{o} C. The supernatant is discarded, and the plates are washed five times with tap water and air dried. Sulforhodamine B (SRB) solution (100 mL) at 0.4% (w/v) in 1% acetic acid is added to each well, and plates are incubated for 10 minutes at room temperature. After staining, unbound dye is removed by washing five times with 1% acetic acid and the plates are air dried. Bound stain is subsequently solubilized with 10 mM trizma base, and the absorbance is read on an automated plate reader at a wavelength of 515 nm. For suspension cells, the methodology is the same except that the assay is terminated by fixing settled cells at the bottom of the wells by gently adding 50 mL of 80% TCA (final concentration, 16% TCA). Using the absorbance measurements [time zero, (Tz), control growth, (C), and test growth in the presence of compound (Ti)], the percentage growth is calculated for each compound. Percentage growth inhibition is calculated as:

[(Ti – Tz)/ (C – Tz)] x100 for concentrations for which Ti >/= Tz.

[(Ti – Tz)/ Tz] x100 for concentrations for which Ti < Tz.

4. 2. 2. Measurement of IC_{50} against ovarian cancer OVCAR-3 and leukemia HL-60 (TB) cell lines

4. 2. 2. 1. Cell Culture

Cell Line cells were obtained from American Type Culture Collection, cells were cultured using Dulbecco's Modified Eagle's medium (DMEM) (Invitrogen / Life Technologies) supplemented with 10% fetal bovine serum (FBS) (Hyclone), 10 μg/mL of insulin (Sigma), and 1% penicillin-streptomycin. All of the other chemicals and reagents were from Sigma, or Invitrogen. Plate cells (cells density 1.2 – 1.8 × 10,000 cells/ well) in a volume of 100μL complete growth medium and 100 μL of the tested compound per well in a 96-well plate for 24 h before the MTT assay.

4. 2. 2. 2. Cell culture protocol

Remove culture medium to a centrifuge tube. Briefly rinse the cell layer with 0.25% (w/v) Trypsin 0.53 μM ethylenediaminetetraacetic acid (EDTA) solution to remove all traces of serum which contains Trypsin inhibitor. Add 2.0 to 3.0 mL of Trypsin EDTA solution to flask and observe cells under an inverted microscope until cell layer is dispersed. Add 6 to 8 mL of complete growth medium and aspirate cells by gently pipetting. Transfer the cell suspension to the centrifuge tube with the medium and centrifuge for 5 to 10 minutes. Discard the supernatant. Resuspend the cell pellet in fresh growth medium. Add appropriate aliquots of the cell suspension to new culture vessels. Incubate cultures at 37°C for 24 h. After treatment of cells with the serial concentrations of the compound to be tested incubation is carried out for 48 h at 37ºC, then the plates are to be examined under the inverted microscope and proceed for the MTT assay.

4. 2. 2. 3. MTT assay protocol

The 3-(4, 5-dimethylthiazol-2-yl)-2,5-diphenyltetrazolium bromide (MTT) method [34] of monitoring *in vitro* cytotoxicity is well suited for use with multiwell plates. The assessment of cell population growth is based on the capability of living cells to reduce the yellow product MTT to a blue product, formazan, by a reduction reaction occurring in the mitochondria. The five cell lines were incubated for 24 h in 96-microwell plates. The number of living cells in the presence or absence (control) of the various test compounds is directly proportional to the intensity of the blue color, measured by spectrophotometry using (ROBONIK P2000 Spectrophotometer) at a wavelength of 570 nm. Measure the background absorbance of multiwell plates at 690 nm and subtract from the 570 nm measurement. Five concentrations ranging from 0.01μM to 100 μM (with semi-log decrease in concentration) were tested for each of the compounds under study. Each experiment was carried out in triplicate. The IC_{50} values [the concentration required for 50% inhibition of cell viability] were calculated using sigmoidal dose response curve-fitting models.

4. 2. 3. Measurement of inhibitory activity against FAK

Compounds **3d**, **3e**, **3f** and **3q** were selected to be evaluated against FAK enzyme using ab187395–FAK Human Simple Step ELISA® Kit according to manufacturer's instructions. In brief, prepare all reagents, working standards, and samples. Add 50 µL of all sample or standard to appropriate wells. Add 50 µL of the antibody cocktail to each well. Seal the plate and incubate for 1 h at room temperature on a plate shaker set to 400 rpm. Wash each well with 3 x 350 µL wash buffer. Wash by aspirating or decanting from wells then dispensing 350 µL wash buffer into each well. Add 100 µL of 3, 3', 5, 5'-Tetramethylbenzidine (TMB)

substrate to each well and incubate for 10 minutes in the dark on a plate shaker set to 400 rpm. Add 100 μL of stop solution to each well. Shake plate on a plate shaker for 1 minute to mix. Record the OD at 450 nm. Subtract average zero standard from all readings. Average the duplicate readings of the positive control dilutions and plot against their concentrations. Draw the best smooth curve through these points to construct a standard curve. Interpolate protein concentrations for unknown samples from the standard curve plotted.

4. 2. 4. Cell-based FAK auto-phosphorylation assay

FAK (Phospho-Tyr397) Cell-Based ELISA Kit was used to monitor FAK protein phosphorylation and expression profile in cells treated with compound **3e** according to manufacturer's instructions. Seed 200 μL of 20,000 adherent cells in culture medium in each well of a 96-well plate. Incubate the cells for overnight at 37°C, 5% CO_2. Remove the cell culture medium and rinse with 200 μLof 1x (Tris Buffered Saline) TBS, twice. Fix the cells by incubating with 100 μL of fixing solution for 20 minutes at room temperature. Remove the fixing solution and wash the plate 3 times with 200 μL 1x wash buffer for five minutes each time. Add 100 μL quenching buffer and incubate for 20 minutes at room temperature. Wash the plate 3 times with 1x wash buffer for 5 minutes at a time. Add 200 μL of blocking buffer and incubate for 1 h at room temperature. Wash 3 times with 200 μL of 1x wash buffer for 5 minutes at a time. Add 50 μL of 1x primary antibodies (Anti-FAK (Phospho-Tyr397) antibody, anti-FAK antibody and/or anti-GAPDH antibody) to the corresponding wells and incubate for 16 h at 4°C.Wash 3 times with 200 μL of 1x wash buffer for 5 minutes at a time. Add 50 μL of 1x secondary antibodies (HRP-Conjugated Anti-Rabbit IgG and/or HRP-Conjugated Anti-Mouse IgG) to corresponding wells and incubate for 1.5 h at room temperature.

Wash 3 times with 200 µL of 1x wash buffer for 5 minutes at a time. Add 50 µL of ready-to-use substrate to each well and incubate for 30 minutes at room temperature. Add 50 µL of stop solution to each well and read OD at 450 nm immediately using the microplate reader.

4. 2. 5. Measurement of inhibitory activity of compound 3e against Pyk2

Compound **3e** was evaluated against Pyk2 using Pyk2 Kinase Assay/Inhibitor Screening Kit according to manufacturer's instructions. In brief, add 100 µL of reaction mixture to the wells. Incubate for 60 minutes at 30°C. Wash the wells. Add 100 µL of (horseradish peroxidase) HRP conjugated anti-phosphotyrosine antibody then incubate for 60 minutes at room temp. Wash the wells. Add 100 µL of substrate reagent. Add 100 µL of stop solution. Measure absorbance at 450 nm.

4. 2. 6. Molecular Docking of the compound 3e

The molecular docking of the compound **3e** was carried out using Molecular Operating Environment (MOE, 10.2008) software. All minimizations were performed with MOE until an RMSD gradient of 0.05 kcal $mol^{-1}A°^{-1}$ with MMFF94x force field and the partial charges were automatically calculated. The X-ray crystallographic structure of FAK PDB (ID: 2ETM) was downloaded from the protein data bank. The receptor was prepared for docking study using Protonate 3D protocol in MOE with default options followed by water molecules removal. The co-crystallized ligand was used to define the active site for docking. Triangle Matcher placement method and London dG scoring function were used for docking. Docking setup was first validated by re-docking of the co-crystallized ligand in the vicinity of the active site of the receptor with energy score (S) = -13.76 kcal/mol. The validated setup was then used in

predicting the ligands receptor interactions at the active site for compound **3e**.

4. 2. 7. Measurement of the effect of compound 3e on the level of caspase-3 protein (Marker of apoptosis):

The level of the apoptotic marker caspase-3 was assessed using BIORAD iScriptTM One-Step RT-PCR kit with SYBR® Green. The procedure of the used kit was done according to the manufacturer's instructions.

4. 2. 7. 1. RNA isolation and reverse transcription:

m RNA isolation is carried out using RNeasy extraction kit, up to 1 x 107 cells, depending on the cell line. Cells are disrupted in RNeasy Lysis Buffer (RLT buffer) and homogenized, ethanol is then added to the lysate, creating conditions that promote selective binding of RNA to the RNeasy membrane. The sample is then applied to the RNeasy Mini spin column, total RNA binds to the membrane, contaminants are efficiently was headway, and high quality RNA is eluted in RNase-free water.

4. 2. 7. 2. Master Mix preparation:

All the following reagents were mixed together to give total volume (50 μL). 2X SYBR® Green RT-PCR reaction mixture (25 μL), forward primer (10 μM) (1.5 μL), reverse primer (10 μM) (1.5 μL), nuclease-free H_2O (11 μL), RNA template (1 pg to 100 ng total RNA) (10 μL) and iScript reverse transcriptase for One-Step RT-PCR (1 μL).

4. 2. 7. 3. Amplification protocol:

Incubate complete reaction mixture in a real-time thermal detection system (Rotorgene) as follows: cDNA synthesis: 10 minutes at 50°C, iScript reverse transcriptase inactivation: 5 minutes at 95°C, polymerase chain reaction (PCR) cycling and detection (30 to 45 cycles): 10 seconds

at 95°C and 30 seconds at 55°C to 60°C (data collection step) and melt curve analysis: 1 minute at 95°C and 1 minute at 55°C and 10 seconds at 55°C (80 cycles, increasing each by 0.5°C each cycle).

4. 2. 8. Cell cycle analysis of compound 3e

The OVCAR-3 cells were treated with compound **3e** at its IC_{50} concentration for 24 h. After treatment, the cells were washed twice with ice-cold phosphate buffer saline (PBS), collected by centrifugation, and fixed in ice-cold 70% (v/v) ethanol, washed with PBS, re-suspended with 0.1 mg/mL RNase, stained with 40 mg/mL propidium iodide (PI), and analyzed by flow cytometry using FACS Calibur (Becton Dickinson) [35]. The cell cycle distributions were calculated using Cell- Quest software (Becton Dickinson). Exposure of OVCAR-3 cells to compound **3e** resulted in an interference with the normal cell cycle distribution as indicated.

4. 2. 9. Measurement of apoptosis using Annexin-V-FITC apoptosis Detection kit

Apoptosis was determined by staining the cells with Annexin V fluorescein isothiocyanate (FITC) and counterstaining with PI using the Annexin V-FITC/PI apoptosis detection kit (BD Biosciences, San Diego, CA) according to the manufacturer's instructions. Briefly, 4×10^6 cell/T 75 flask were exposed to compound **3e** at its IC_{50} concentration for 24 h. The cells then were collected by trypsinization and 0.5×10^6 cells were washed twice with PBS and stained with 5 μL Annexin V-FITC and 5 μL PI in 1×binding buffer for 15 minutes at room temperature in the dark. Analyses were performed using FACS Calibur flow cytometer (BD Biosciences, San Jose, CA).

Acknowledgments

The authors are grateful to all members of National Institute of Health, Meryland, USA for carrying out the anticancer screening. The authors thank Dr. Esam Rashwan, Head of the confirmatory diagnostic unit VACSERA-EGYPT, for carrying out the cytotoxicity testing, cell cycle analysis, active caspase-3 and *in vitro* FAK and Pyk2 inhibition assays.

References

[1] Y. Lazebnik, What are the hallmarks of cancer?, Nat. Rev. Cancer 10 (2010) 232–233.

[2] Y. Sonoda, S. Watanabe, Y. Matsumoto, E. Aizu-Yokota, T. Kasahara, FAK is the upstream signal protein of the phosphatidylinositol 3-kinase-Akt survival pathway in hydrogen peroxide-induced apoptosis of a human glioblastoma cell line, J. Biol. Chem. 274 (1999)10566-10570.

[3] S. Hiscox, P. Barnfather, E. Hayes, P. Bramble, J. Christensen, R. I. Nicholson, P. Barrett-Lee, Inhibition of focal adhesion kinase suppresses the adverse phenotype of endocrine-resistant breast cancer cells and improves endocrine response in endocrine-sensitive cells, Breast Cancer Res. Treat. 125 (2011) 659- 669.

[4] M. J. van Nimwegen, B. van de Water, Focal adhesion kinase: A potential target in cancer therapy, Biochem. Pharmacol. 73(2007) 597-609.

[5] Y. Sonoda, Y.Matsumoto, M.Funakoshi, D. Yamamoto, S K. Hanks, ,T. Kasahara, Anti-apoptotic Role of Focal Adhesion Kinase (FAK), J. Biol. Chem. 275(2000) 16309–16315.

[6] V. Gabarra-Niecko, M. D. Schaller, J. M. Dunty, FAK regulates biological processes important for the pathogenesis of cancer, Cancer Metastasis Rev. 22 (2003) 359–374.

[7] Cancer Genome Atlas Research Network: Integrated genomic analyses of ovarian carcinoma. Nature 474 (2011) 609-615.

[8] H. Okamoto, K. Yasui, C. Zhao, S. Arii, J. Inazawa, PTK2 and EIF3S3 genes may be amplification targets at 8q23-q24 and are associated with large hepatocellular carcinomas, Hepatology 38 (2003) 1242-1249.

[9] G. W. McLean, N. O. Carragher, E. Avizienyte, J. Evans, V. G.

Brunton, M. C. Frame, The role of focal adhesion kinase in cancer, a new therapeutic opportunity, Nat. Rev. Cancer 5 (2005) 505–515.

[10] A. Schultze, W. Fiedler, Therapeutic potential and limitations of new FAK inhibitors in the treatment of cancer, Expert Opin. Investig. Drugs 19 (2010)777-788.

[11] J. Schwock, N. Dhani, D.W. Hedley, Targeting focal adhesion kinase signaling in tumor growth and metastasis, Expert Opin. Ther. Targets 14 (2010) 77-94.

[12] M. A. Cabritaa, L.M. Jonesa, J. L. Quizia, L A. Sabourina , B. C. McKaya , C. L. Addisona, Focal adhesion kinase inhibitors are potent anti-angiogenic agents, Mol. Oncol. 5 (2011) 517 -526.

[13] P. E. Goss, Pre-clinical and clinical review of vorozole, a new third generation aromatase inhibitor, Breast Cancer Res. Treat. 49 (1998) 59-65.

[14] J. S. Duncan, L. Gyenis, J. Lenehan, M. Britney, L. M. Graves, T. A. Haystead, D. W. Litchfield, An unbiased evaluation of CK2 inhibitors by

chemoproteomics: characterization of inhibitor effects on CK2 and identification of novel inhibitor targets, Mol. Cell Proteomics 7 (2008) 1077-1088.

[15] Y. Luo, Z. Liu, G. Chen, J. Shi, J. Lia, H. Zhu, 1,3,4-Oxadiazole derivatives as potential antitumor agents: discovery, optimization and biological activity valuation, Med. Chem. Commun. 7(2016) 263-271.

[16] S. Zhang, Y. Luo, L.He, Z.Liu, A. Jiang, Y.Yang, H. Zhu, Synthesis, biological evaluation, and molecular docking studies of novel 1,3,4-oxadiazole derivatives possessing benzotriazole moiety as FAK inhibitors with anticancer activity, Bioorganic Med. Chem. 21 (2013) 3723–3729.

[17] R.R. Hantgan, M.C. Stahle, Integrin priming dynamics: Mechanisms of integrin antagonist-promoted αIIbβ3· PAC-1 molecular recognition, Biochemistry 48 (2009) 8355-8365.

[18] Z. Liang, D. Zhang, J. Ai, L. Chen, H. Wang, X. Kong, M. Zheng, H. Liu, C. Luo, M. Geng, H. Jiang, K. Chen, Identification and synthesis of *N′*-(2-oxoindolin-3-ylidene)hydrazide derivatives against c-Met kinase, Bioorg. Med. Chem. Lett. 21 (2011) 3749-3754.

[19] D.C. Hsu, H.S. Roth, D.C. West, R.C. Botham, C.J. Novotny, S.C. Schmid, P.J. Hergenrother, Parallel synthesis and biological evaluation of 837 analogues of procaspase-activating compound 1 (PAC-1), ACS Comb. Sci. 14 (2012) 44-50.

[20] L. K. Charkoudian, D. M. Pham, K. J. Franz, A pro-chelator triggered by hydrogen peroxide inhibits iron-promoted hydroxyl radical formation, J. Am. Chem. Soc. 128 (2006) 12424−12425.

[21] Q. P. Peterson, D. C. Hsu, D. R. Goode, C. J. Novotny, R. K. Totten, P. J. Hergenrother, Procaspase-3 activation as an anticancer

strategy: Structure−activity relationship of procaspase-activating compound 1 (PAC-1) and its cellular co-localization with caspase-3, J. Med. Chem. 52 (2009) 5721−5731.

[22] Q. P. Peterson, D. R. Goode, D. C. West, K. N. Ramsey, J. J. Y. Lee, P. J. Hergenrother, PAC-1 activates procaspase-3 in vitro through relief of zinc-mediated inhibition, J. Mol. Biol. 388 (2009) 144−158.

[23] R. Morphy, Z. Rankovic, Designed multiple ligands. An emerging drug discovery paradigm, J. Med. Chem. 48 (2005) 6523-6543.

[24] A.L. Hopkins, Network pharmacology: the next paradigm in drug discovery, Nat. Chem. Biol. 4 (2008) 682-690.

[25] T. Mitchell, M. Cherry, Fragment-based drug design, Innov. Pharm. Technol. 16 (2005) 34-36.

[26] D. Erlanson, R. S. McDowell, T. O'Brien, Fragment-based drug discovery, J. Med. Chem. 47 (2004) 3463–3482.

[27] M. Getlik, C. Grütter, J. R. Simard, S. Klüter, M. Rabiller, H. B. Rode, A. Robubi, D. Rauh, Hybrid compound design to overcome the gatekeeper T338M mutation in cSrc, J. Med. Chem. 52 (2009) 3915-3926.

[28] P. Kumar, L. Tripathi, A new class of anticonvulsants possessing 6 Hz psychomotor seizure test activity: 2-(1H-Benzotriazol-1-yl)-N'-[substituted] acetohydrazides, Med. Chem. 8 (2012) 337-348.

[29] O. M. Ali, A. E. G. E. Amr, E. E. Mostafa, Synthesis and antimicrobial of some new substituted tetrazolomethylbenzo[*d*]-[1,2,3]triazole derivatives using 1H-benzo[*d*][1,2,3]triazole as starting material, Res. Chem. Intermed. 40 (2014) 1545-1556.

[30] I. Vermes, C. Haanen, H. Steffens-Nakken, C. J. A Reutelingsperger, A novel assay for apoptosis Flow cytometric detection of phosphatidylserine early apoptotic cells using fluorescein labelled expression on Annexin V, J. Immunol. Methods. 184 (1995) 39-51.

[31] M. C. Alley, D. A. Scudiero, P. A. Monks, M. L. Hursey, M. J., Fine, D. L. Czerwinski, B. J. Abbott, J. G. Mayo, R. H. Shoemaker, M. R. Boyd, Feasibility of drug screening with panels of human tumor cell lines using a microculture tetrazolium assay, Cancer Res. 48 (1988) 589-601.

[32] M. R. Grever, S. A. Schepartz, B. A. Chabner, The National Cancer Institute: cancer drug discovery and development program, Semin. Oncol. 19 (1992) 622-638.

[33] M. R. Boyd, K. D. Paull, Some practical considerations and applications of the national cancer institute in vitro anticancer drug discovery screen, Drug Develop. Res. 34 (1995) 91-109.

[34] T. Mosmann, Rapid colorimetric assay for cellular growth and survival: Application to proliferation and cytotoxicity assays, J. Immunol. Methods, 65 (1983) 55-63.

[35] M. F. Tolba, A. Esmat, A. M. Al-Abd, S. S. Azab, A. E. Khalifa, H. A. Mosli, S. Z. Abdel-Rahman, A. B. Abdel-Naim, Caffeic acid phenethyl ester synergistically enhances docetaxel and paclitaxel cytotoxicity in prostate cancer cells, Int. Union Biochem. Mol. Biol. 65 (2013) 716–729.

Figure 1. Structures of potent anticancer drugs and FAK inhibitors and design strategy for the target benzotriazole N-acylarylhydrazone hybrids.

Figure 2. Tautomerism in benzotriazole N-acylarylhydrazone hybrids **3a-3q**.

Figure 3. Graphical representation for concentrations required for 50% inhibition of cell viability (IC_{50}) of compounds **3d**, **3e**, **3f** and **3q** compared to doxorubicin.

Figure 4. Graphical representation for the concentrations required for 50% inhibition of FAK enzyme (IC_{50}) of compounds **3d**, **3e**, **3f** and **3q** compared to GSK-2256098.

Figure 5. Line representation of the effect of compound **3e** on FAK enzyme.

Figure 6. The 2D interaction of compound **3e** with the amino acids of the active site of FAK.

Figure 7. The 3D interaction of compound **3e** with the amino acids of the active site of FAK.

Figure 8. Graphical representation for active caspase-3 assay of compounds **3e** compared to doxorubicin.

Figure 9. Effect of compound **3e** (0.029μM) on DNA-ploidy flow cytometric analysis of OVCAR-3cells after 24 h.

Figure 10. Graphical representation of the cell cycle analysis of compound **3e**.

Figure 11. Representative dot plots of OVCAR-3 cells treated with **3e** (0.029μM) for 24 h and analyzed by flow cytometry after double staining of the cells with annexin-V FITC and PI.

Figure 12. Graphical representation of effect of compound **3e** on apoptosis and necrosis.

Scheme 1. The synthetic path and reagents for the preparation of the target benzotriazole N-acylarylhydrazone hybrids **3a-q**.

Table 1. Growth inhibition percentages obtained from the single dose (10^{-5}M) test.

Table 2. Concentrations required for 50% inhibition of cell viability (IC_{50}) of compounds **3d**, **3e**, **3f** and **3q** compared to doxorubicin.

Table 3. Concentrations required for 50% inhibition of FAK enzyme (IC_{50}) of compounds **3d**, **3e**, **3f** and **3q** compared to GSK-2256098.

Table 4. Effect of compound **3e** on caspase-3 compared to doxorubicin.

Table 5. Cell cycle distribution of compound **3e**.

Table 6. Effect of compound **3e** on apoptosis and necrosis.

Table 1.Growth inhibition percentages obtained from the single dose (10^{-5}M) test.

Panel/ cell line	Compound				
	3d	**3e**	**3f**	**3o**	**3q**
Leukemia					
CCRF-CEM	**64.24**	**86.69**	**66.08**	17.12	**52.29**
HL-60(TB)	19.30	**86.42**	34.88	-1.24	**68.87**
K-562	20.80	**54.43**	30.76	**64.72**	**84.79**
MOLT-4	43.73	**74.19**	**62.47**	16.91	**70.08**
RPMI-8226	29.96	**52.39**	18.61	17.41	**54.99**

SR	**56.93**	**70.45**	**64.37**	**62.07**	**81.66**
Non-Small Cell Lung Cancer					
A549/ATCC	35.77	24.24	42.22	38.01	**51.00**
EKVX	23.78	32.26	35.49	21.65	37.65
HOP-62	**51.80**	**60.39**	**64.81**	34.54	**63.43**
HOP-92	15.32	18.52	16.69	28.18	42.30
NCI-H226	13.36	19.20	21.99	13.88	23.02
NCI-H23	22.81	30.85	19.85	15.03	29.00
NCI-H322M	41.96	41.23	**50.61**	7.92	20.02
NCI-H460	**60.77**	**66.97**	**63.54**	31.67	**79.03**
NCI-H522	21.66	**54.36**	32.08	**68.00**	**81.88**
Colon Cancer					
COLO 205	42.74	47.07	**75.23**	42.44	**62.84**
HCC-2998	27.79	24.38	35.65	9.68	21.20
HCT-116	37.12	**53.34**	42.87	40.17	**73.06**
HCT-15	**70.14**	**74.21**	**67.85**	**62.26**	**66.75**
HT29	9.99	22.58	47.70	**68.76**	**86.86**
KM12	**51.23**	**51.94**	**54.14**	**55.37**	**77.39**
SW-620	34.74	**50.16**	36.95	**52.56**	**74.67**
CNS Cancer					
SF-268	46.16	**60.62**	47.07	12.46	42.50
SF-295	34.13	43.55	**54.41**	28.70	**55.56**
SF-593	16.56	47.10	32.41	3.41	48.13
SNB-19	31.25	46.58	38.12	18.36	**58.68**
SNB-75	20.92	35.23	35.18	31.28	**66.45**
U251	49.46	**65.98**	**60.42**	21.89	**60.50**
Melanoma					
LOX IMVI	**52.23**	**77.62**	**61.00**	22.44	**53.93**
MALME-3M	0.15	30.77	9.61	25.76	39.00
M14	35.22	**51.24**	43.48	37.81	**80.26**
MDA-MB-435	20.52	35.14	25.71	**80.89**	**115.92**
SK-MEL-2	16.68	18.65	18.45	24.93	**61.59**
SK-MEL-28	32.24	32.82	35.78	14.85	27.48
SK-MEL-5	31.46	44.69	33.86	33.29	**71.56**
UACC-257	17.81	22.68	10.67	7.57	34.69
UACC-62	**51.33**	**64.89**	**59.09**	43.97	**76.99**
Ovarian Cancer					
IGROV1	36.25	30.92	38.45	46.19	45.94
OVCAR-3	**71.17**	**78.24**	**74.00**	26.06	**77.60**
OVCAR-4	40.35	49.70	46.87	16.33	19.95
OVCAR-5	29.03	22.98	29.31	4.11	28.14
OVCAR-8	39.62	**57.77**	47.18	20.74	**55.22**
NCI/ADR-RES	44.36	**70.68**	40.01	48.95	**52.44**
SK-OV-3	46.36	30.90	**64.77**	13.50	34.29
Renal Cancer					
786-0	32.24	47.93	37.18	5.60	42.03
A498	20.09	8.01	22.16	16.92	39.65
ACHN	49.53	**73.77**	**51.27**	18.07	35.89

Table 1 (continued)

Panel/ cell line	**Compound**				
	3d	**3e**	**3f**	**3o**	**3q**
CAKI-1	**65.54**	**55.67**	**63.02**	46.48	**54.27**
RXF 393	16.34	24.70	21.87	6.21	33.45
SN12C	32.05	44.79	29.64	16.37	**54.06**
TK-10	35.47	26.45	38.87	16.02	35.30
UO-31	**70.10**	**83.14**	**61.97**	39.09	47.59

Prostate Cancer					
PC-3	34.98	43.99	42.32	28.09	38.31
DU-145	29.52	43.40	37.95	-4.31	19.04
Breast Cancer					
MCF7	45.00	**69.66**	47.07	**69.27**	**77.99**
MDA-MB-231/ATCC	30.98	36.10	38.55	21.53	47.97
HS 578T	24.39	27.17	28.64	34.51	42.45
BT-549	19.09	37.92	23.90	17.14	47.57
T-47D	43.12	39.65	27.49	19.41	**62.92**
MDA-MB-468	18.45	24.21	21.74	-4.69	**65.52**

Table 2 Concentrations required for 50% inhibition of cell viability (IC_{50}) of compounds **3d**, **3e**, **3f** and **3q** compared to doxorubicin.

	IC_{50} (μM*±SD)	
Compound	OVCAR-3	HL-60(TB)
3d	0.130±0.006	N.T.
3e	0.029±0.001	0.025±0.002
3f	0.037±0.002	N.T.
3q	0.028±0.003	N.T.
Doxorubicin	0.300±0.010	0.450±0.010

*The values given are means of three experiments.
HL-60 (TB); leukemia and OVCAR-3; ovarian cancer.
N.T.: not tested.

Table 3. Concentrations required for 50% inhibition of FAK enzyme (IC_{50}) of compounds **3d**, **3e**, **3f** and **3q** compared to GSK-2256098.

Compound	IC_{50} (nM*±SD)
3d	119.22 ± 8.54
3e	44.6 ±2.28
3f	69.2 ±3.15
3q	80.75 ± 3.91
GSK-2256098	39.66 ±1.79

*The values given are means of three experiments.

Table 4. Effect of compound **3e** on caspase-3 compared to doxorubicin.

Compound	**Caspase3 conc.** (Pg/mL*)
3e	541.2±4.26
Doxorubicin	358.9±1.45
Cont.Ovcar-3	47.66±7.12

*The values given are means ± SD of three experiments.

Table 5. Cell cycle distribution of compound **3e**.

Compound	**Cell cycle distribution**			
	%G0/G1	**%S**	**%G2/M**	**%Apoptosis**
3e	26.39	15.37	58.24	24.16
Cont.Ovcar-3	59.36	29.02	11.62	1.71

Table 6. Effect of compound **3e** on apoptosis and necrosis.

Compound	**%Apoptosis**			**%Necrosis**
	Total	**Early**	**Late**	
3e	24.16	6.55	14.83	2.78
Cont.Ovcar-3	1.71	0.41	0.23	1.07

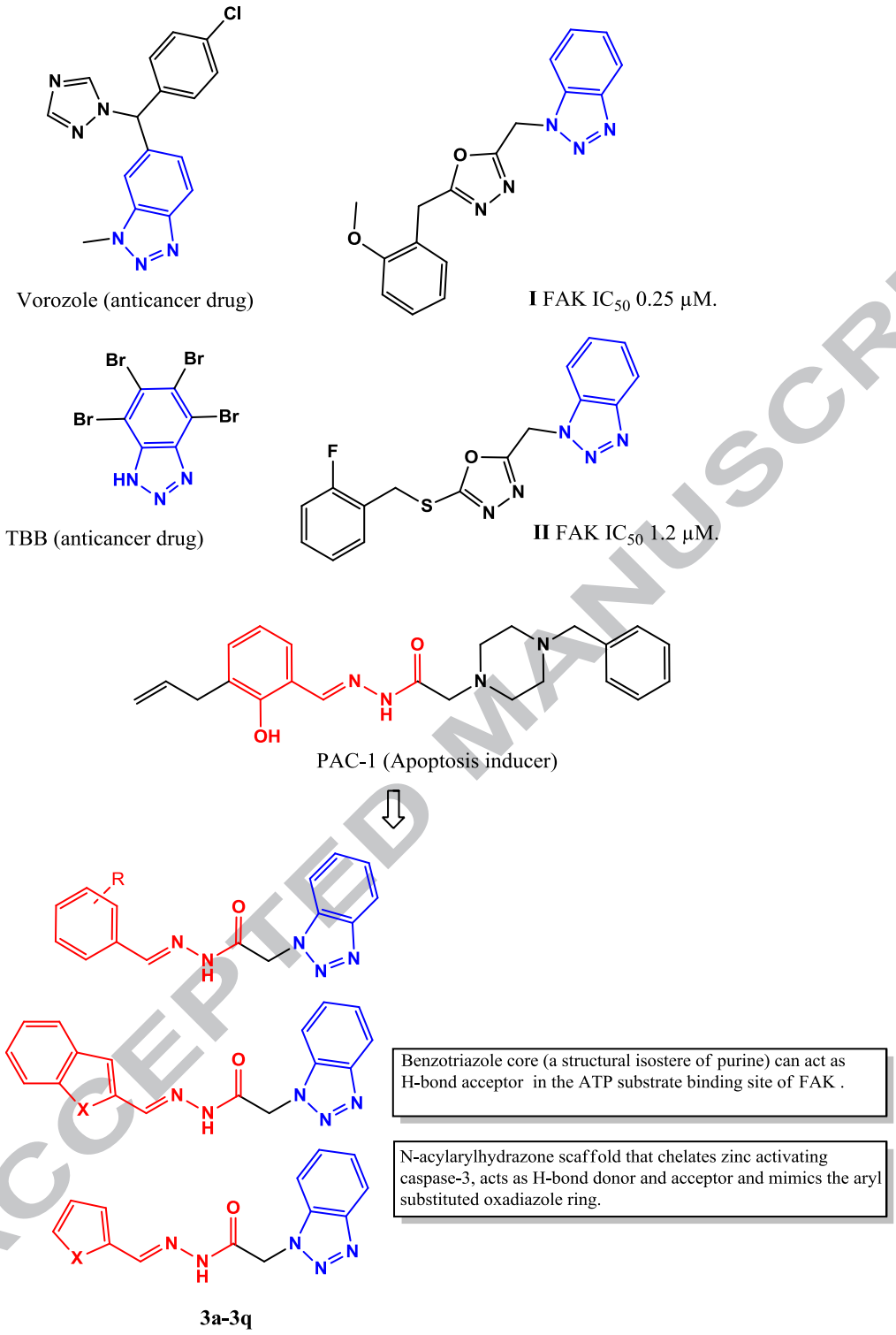

Figure 1. Structures of potent anticancer drugs and FAK inhibitors and design strategy for the target benzotriazole N-acylarylhydrazone hybrids.

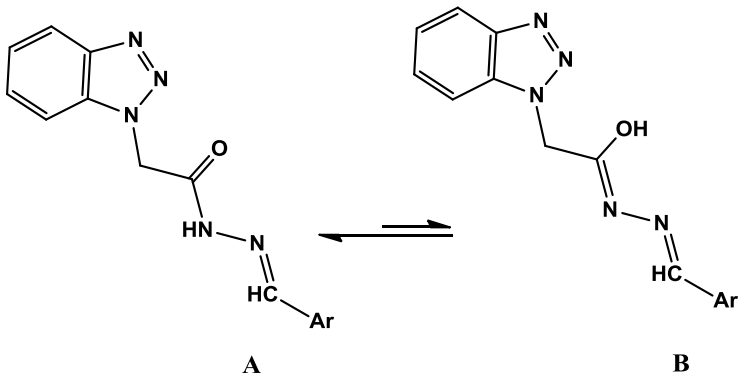

Figure 2. Tautomerism in benzotriazole N-acylarylhydrazone hybrids **3a-3q**.

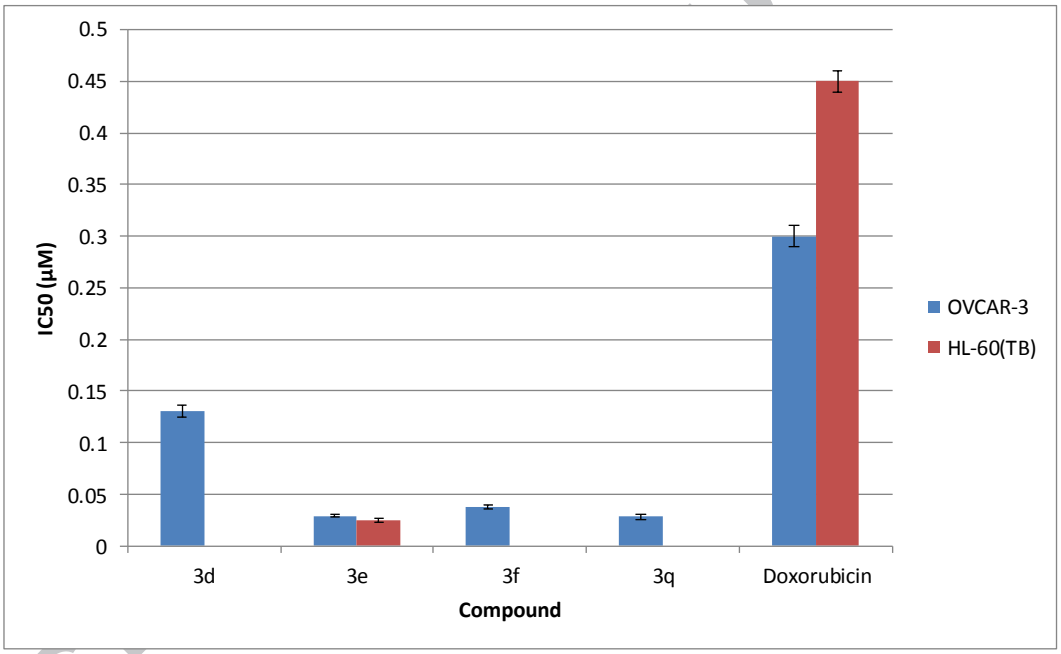

Figure 3. Graphical representation for concentrations required for 50% inhibition of cell viability (IC_{50}) of compounds **3d**, **3e**, **3f** and **3q** compared to doxorubicin.

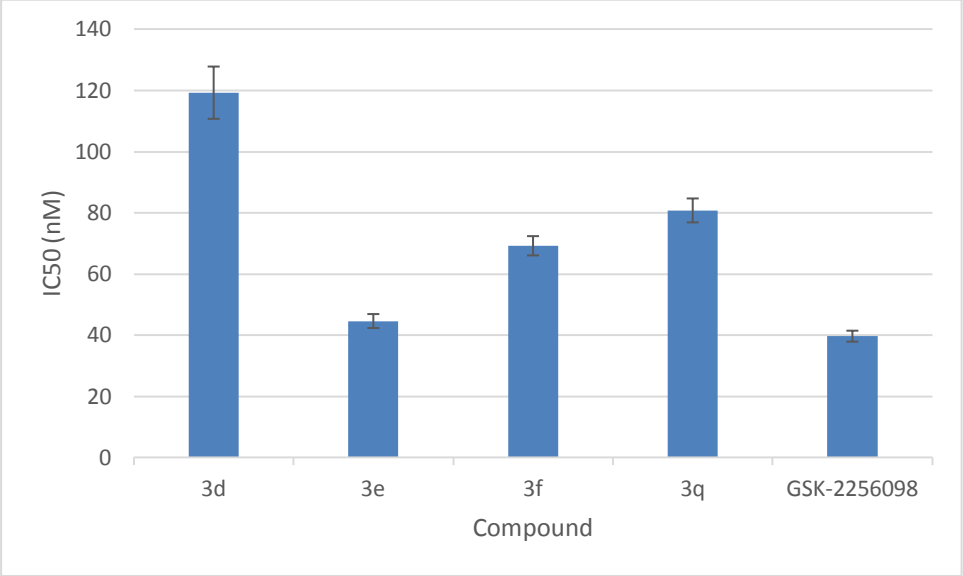

Figure 4. Graphical representation for the concentrations required for 50% inhibition of FAK enzyme (IC_{50}) of compounds **3d**, **3e**, **3f** and **3q** compared to GSK-2256098.

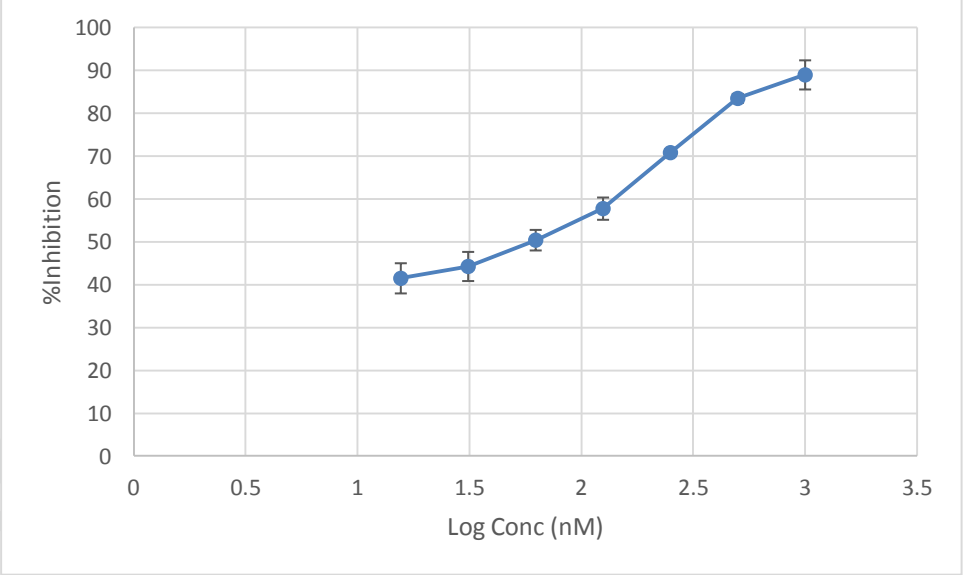

Figure 5. Line representation of the effect of compound **3e** on FAK enzyme.

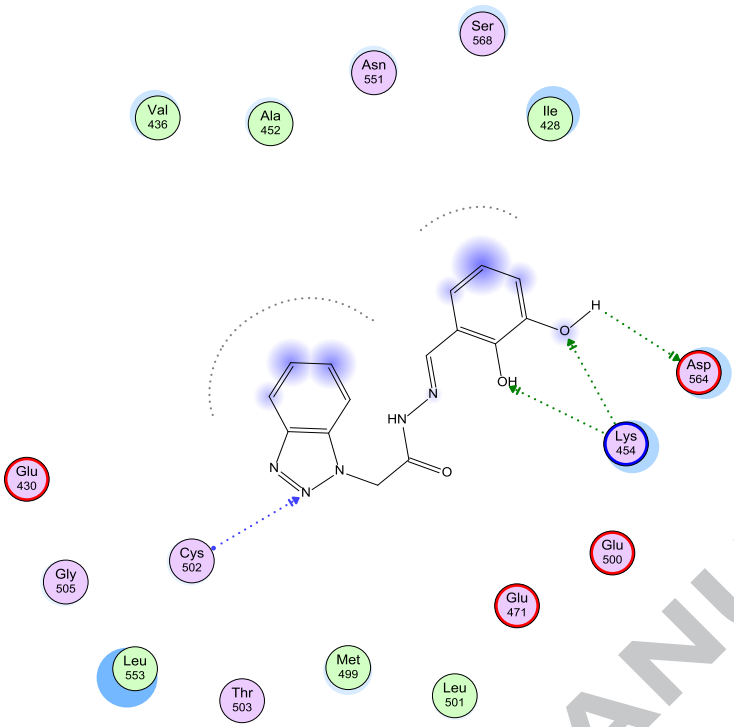

Figure 6. The 2D interaction of compound **3e** with the amino acids of the active site of FAK.

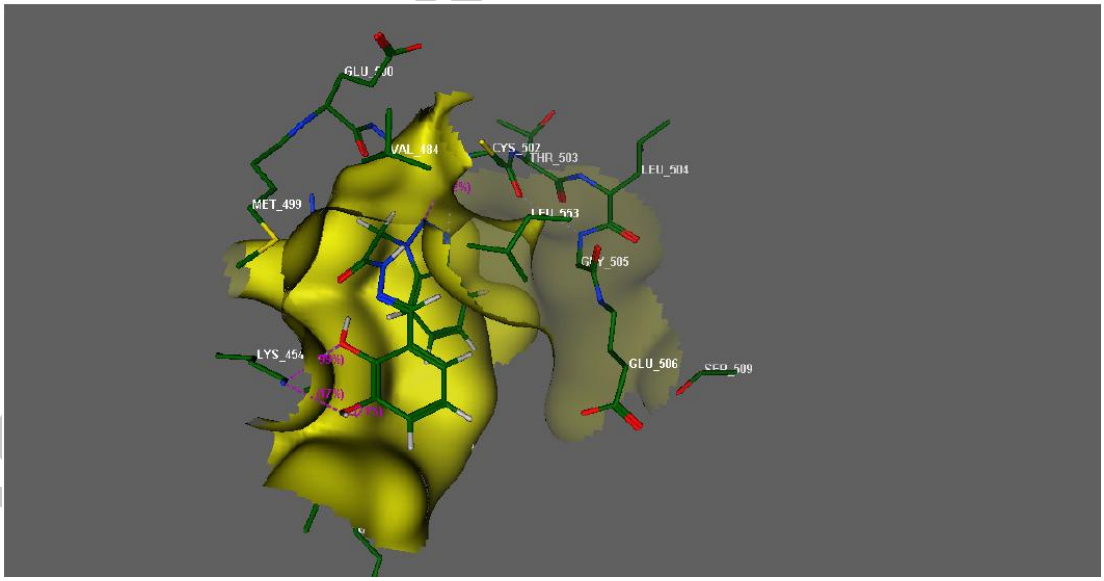

Figure 7. The 3D interaction of compound **3e** with the amino acids of the active site of FAK.

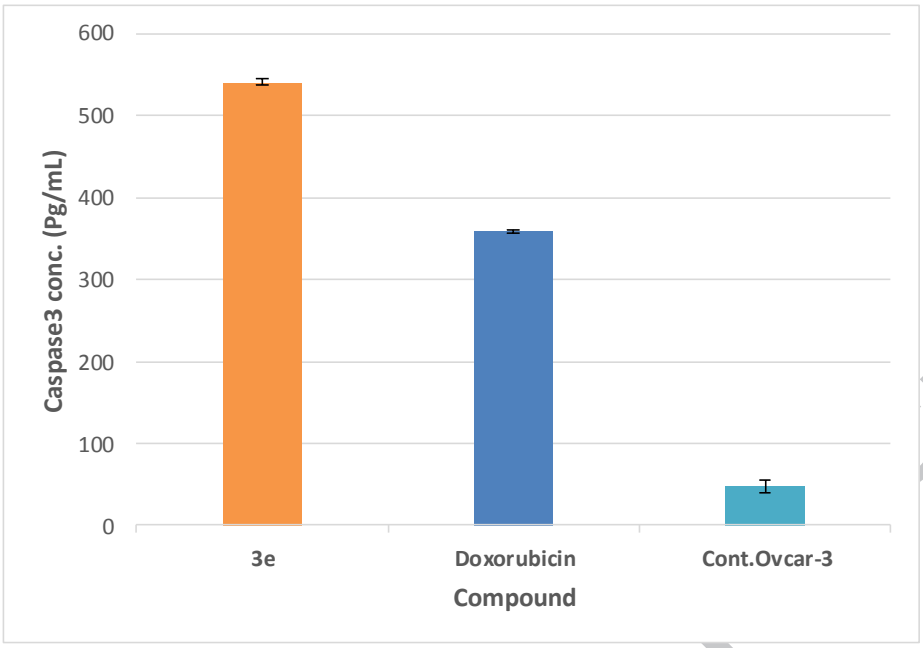

Figure 8. Graphical representation for active caspase-3 assay of compounds **3e** compared to doxorubicin.

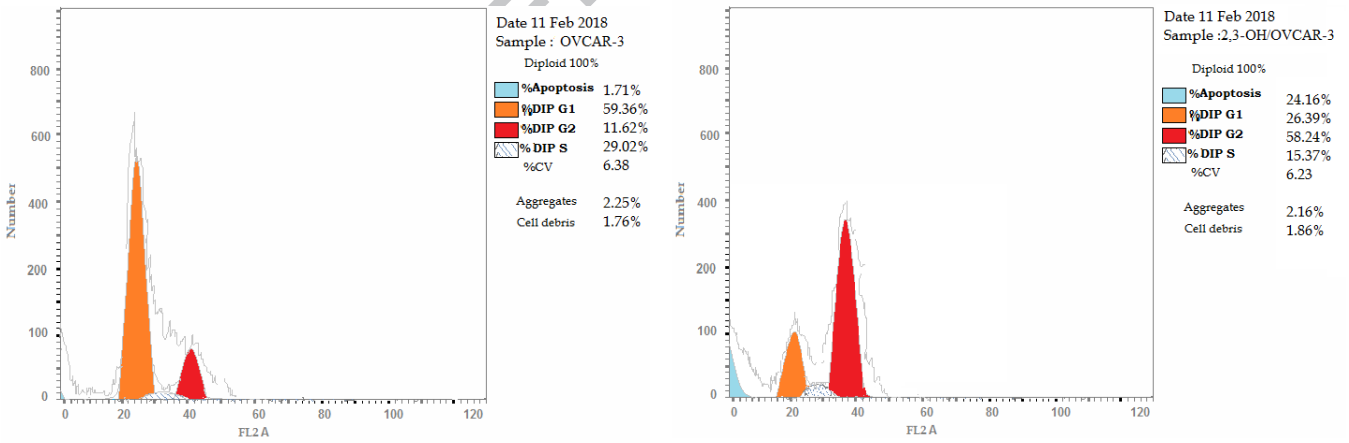

Control **3e**

Figure 9. Effect of compound **3e** (0.029μM) on DNA-ploidy flow cytometric analysis of OVCAR-3cells after 24 h.

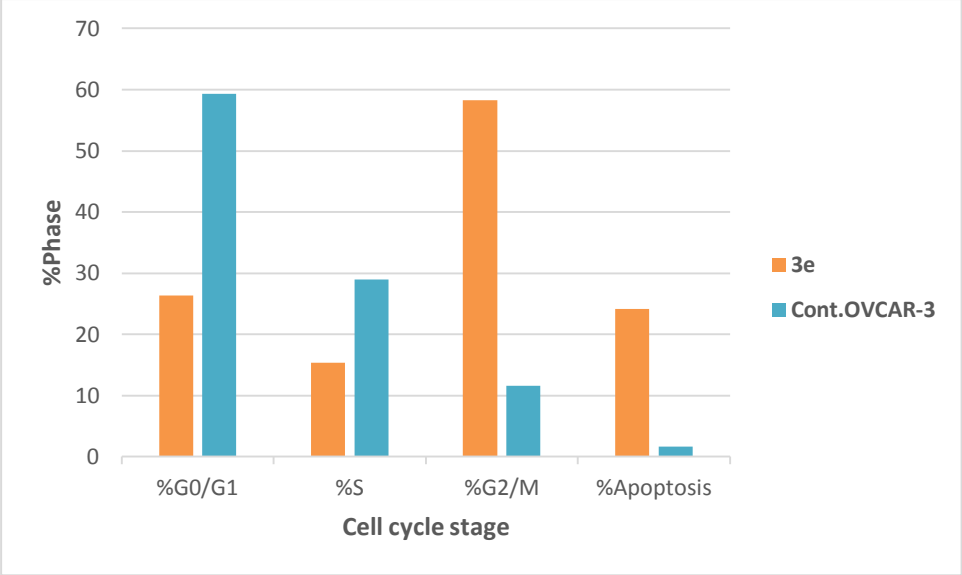

Figure 10. Graphical representation of the cell cycle analysis of compound **3e**.

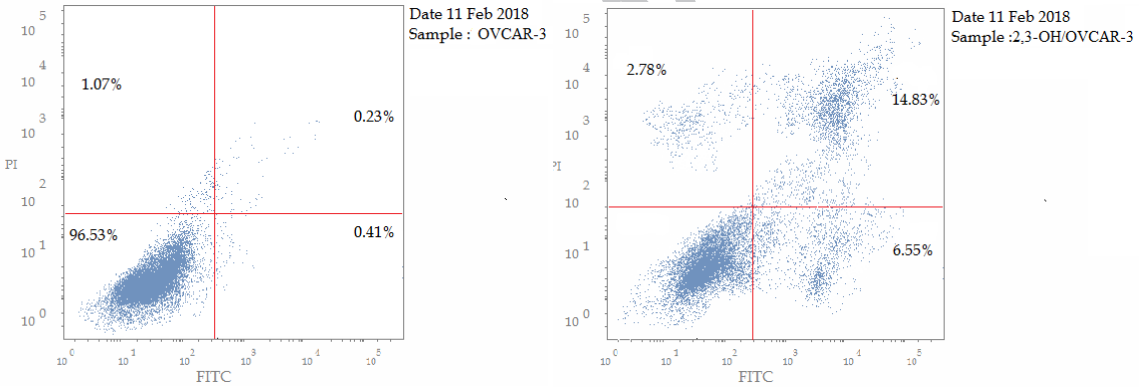

Control **3e**

Figure 11. Representative dot plots of OVCAR-3 cells treated with **3e** (0.029μM) for 24 h and analyzed by flow cytometry after double staining of the cells with annexin-V FITC and PI.

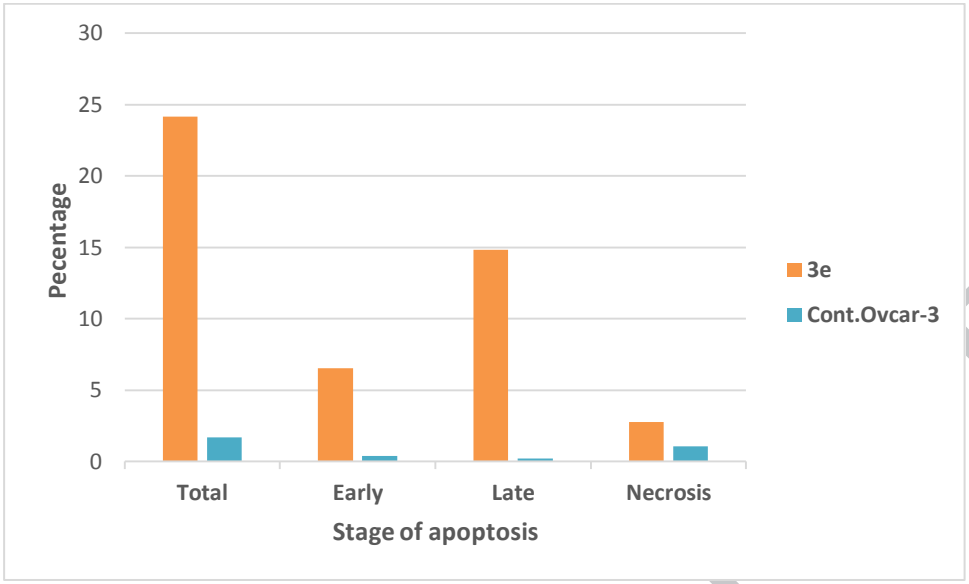

Figure 12. Graphical representation of effect of compound **3e** on apoptosis and necrosis.

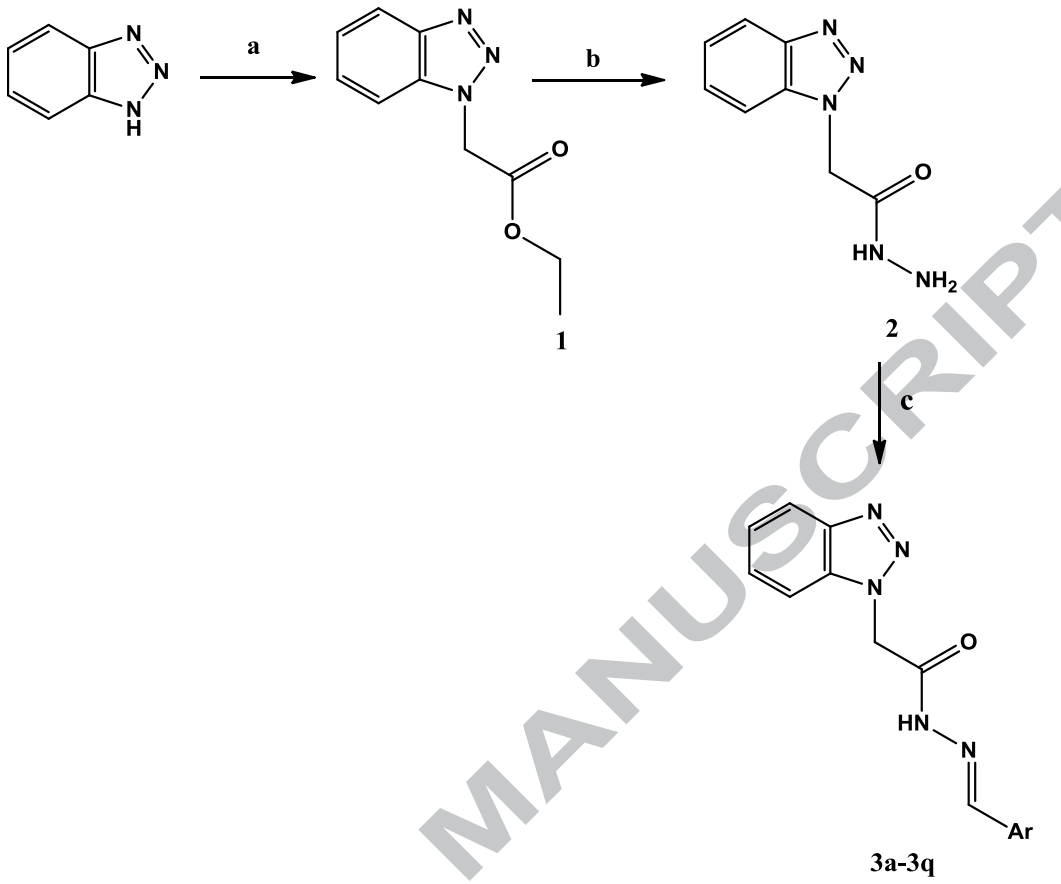

3a: Ar = 2-fluorophenyl
3b: Ar = 3-fluorophenyl
3c: Ar = 4-fluorophenyl
3d: Ar = 2-hydroxyphenyl
3e: Ar = 2,3-dihydroxyphenyl
3f: Ar = 2,4-dihydroxyphenyl
3g: Ar = 3,4-dihydroxyphenyl
3h: Ar =4-methoxyphenyl
3i: Ar = 4-hydroxy-3-methoxyphenyl
3j: Ar = 3,4,5-trimethoxyphenyl
3k: Ar = furan-2-yl
3l: Ar = pyrrol-2-yl
3m:Ar = pyridin-4-yl
3n: Ar = benzofuran-2-yl
3o: Ar = benzothiophen-2-yl
3p: Ar = indol-2-yl
3q: Ar = indol-3-yl

Reagents and conditions: **a)** $ClCH_2COOC_2H_5$, anhyd. K_2CO_3, dry acetone, Reflux 8h; **b)** hydrazine hydrate, ethanol, Reflux 5h, **c)** ArCHO, ethanol, GAA, Reflux 6h.

Scheme 1. The synthetic path and reagents for the preparation of the target benzotriazole N-acylarylhydrazone hybrids **3a-q**.

Graphical abstract

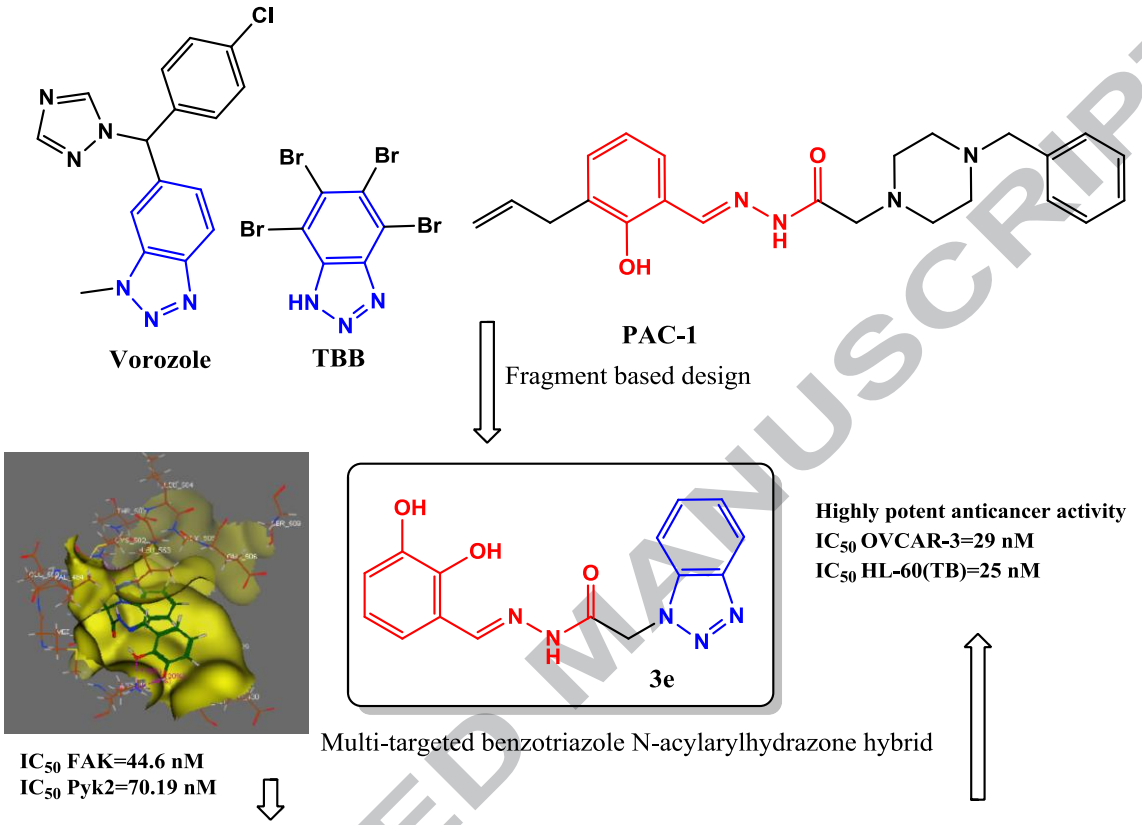

Highlights

- A series of benzotriazole N-acylarylhydrazone hybrids was synthesized.
- The anticancer activity of the new hybrids was tested *in vitro*.
- Multi-targeted potent anticancer hybrid **3e** was identified (IC_{50}= 29, 25 nM).
- Compound **3e** inhibited FAK at nanomolar range (IC_{50} =44.6 nM).
- Compound **3e** increased level of active caspase-3 (11.35 folds).